lubricants

MDPI

Article

A Digital Twin-Driven Method for Predicting the Precision Remaining Useful Life of CNC Rotary Tables

Zongyi Mu [1,2], Hongwei Wang [2,*], Fajuan Xiao [2] and Genbao Zhang [3]

[1] College of Aerospace Engineering, Chongqing University, Chongqing 400044, China
[2] College of Intelligent Manufacturing Engineering, Chongqing University of Arts and Sciences, Chongqing 402160, China
[3] School of Intelligent Manufacturing Engineering, Chongqing Vocational College of Light Industry, Chongqing 400065, China
* Correspondence: 20230046@cqwu.edu.cn; Tel.: +86-13282727207

Abstract

As a core component enabling multi-axis precision machining in CNC machine tools, the CNC rotary table's precision state directly affects machining quality and production efficiency. Real-time and accurate prediction of its precision remaining useful life (PRUL) is of great significance for optimizing maintenance costs, ensuring production safety, and extending equipment service life. To this end, a digital twin framework for PRUL prediction of CNC rotary tables was first established, defining a five-dimensional digital twin model. Then, based on the Meta-action theory, an initial precision model of the CNC rotary table was constructed. Time-varying errors were quantitatively characterized using thermal error simulation and the wear model, and combined with the Wiener process model, theoretical PRUL prediction within the virtual mirror was realized. Finally, the virtual mirror data and physical entity data were fused to generate corrected model parameters, yielding a real-time PRUL prediction model for the CNC rotary table driven by digital twin data. The case study results demonstrate that the proposed method, which integrates the mechanistic model with real-time data, achieves an improvement of at least 16% in both prediction accuracy and stability compared to methods based solely on either virtual mirror data or monitoring data.

Keywords: CNC rotary table; precision remaining useful life; digital twin; Meta-action; wear

1. Introduction

High-end equipment manufacturing serves as a cornerstone of industrial modernization. As a critical functional component of high-end CNC machine tools, the computer numerical control (CNC) rotary table provides additional rotational degrees of freedom through indexing positioning and continuous rotary motion, making it a core actuating unit for multi-axis machining [1]. Its accuracy directly determines the geometric precision and surface quality of complex components such as turbine blades and aerospace structural parts. With the continuously increasing demands for machining quality and efficiency, the accuracy of CNC rotary tables has become one of the key bottlenecks constraining the production stability. Therefore, determining an appropriate maintenance schedule for CNC rotary tables is of great significance for ensuring the machining quality.

Precision remaining useful life (PRUL) refers to the remaining time before the output accuracy of the equipment reaches the precision failure threshold at a given moment. Accurate PRUL prediction can provide quantitative support for maintenance planning,

Check for updates

Received: 4 August 2026
Revised: 26 September 2026
Accepted: 30 September 2026
Published: 1 October 2026

Copyright: © 2026 by the authors. Licensee MDPI, Basel, Switzerland. This article is an open access article distributed under the terms and conditions of the Creative Commons Attribution (CC BY) license.

maximizing component utilization and reducing operational costs while avoiding unexpected downtime. Therefore, for CNC rotary tables, accurate PRUL prediction facilitates the transition of maintenance strategies from reactive repair to proactive maintenance [2], thereby providing strong support for improving overall equipment effectiveness, reducing failure risk and maintenance costs.

However, during long-term operation, multiple coupled factors such as assembly error accumulation, component wear and thermal deformation interact with one another, causing the positioning accuracy of the rotary table to exhibit complex nonlinear degradation characteristics. The degradation process is characterized by time-variance, randomness and multi-stage behavior, and cross-coupling effects exist among different degradation mechanisms, making it difficult to accurately describe the degradation law of rotary table positioning accuracy. Furthermore, factors such as load fluctuations, temperature variations and changes in lubrication conditions under actual operating conditions further exacerbate the uncertainty of the degradation process. The above complexities pose significant challenges to the accurate prediction of the PRUL of CNC rotary tables.

Currently, PRUL prediction methods can be mainly categorized into three types: model-driven theoretical prediction, data-driven real-time prediction and hybrid-driven fusion prediction.

Model-driven approaches primarily rely on physical empirical models—such as the Paris crack propagation model [3], the Coffin–Manson fatigue failure model [4], the Corten–Dolan fatigue damage model [5] and the Archard wear model [6]—to establish theoretical performance degradation curves for electromechanical systems, thereby enabling PRUL prediction. Chang et al. [7] proposed a degradation modeling method for axial piston pumps that integrates operational data with a physics-of-failure model, achieving high-precision remaining useful life (RUL) prediction through feature fusion and Unscented Kalman Filter (UKF)-based parameter updating. Chen et al. [8] presented a spatio-temporal MLP model incorporating physical–informational neural networks for RUL prediction. A gated attention spatio-temporal MLP reduces model complexity, while a fused loss model of lifespan and physical information guides optimization toward physical consistency, improving accuracy under complex operating conditions. Ma et al. [9] proposed a simultaneous six-DOF error measurement method for rotary axes using a polyhedral prism, designed an error-sensitive unit with a prism and reflector, established a mathematical model covering geometric, manufacturing and sensor errors, and experimentally validated the compensation model.

Data-driven approaches, by contrast, analyze real-time collected data using stochastic process models [10], long short-term memory networks (LSTMs) [11], deep learning [12], etc., to fit the patterns of performance degradation and thus predict the PRUL. Liu et al. [13] proposed a self-data-driven remaining useful life (RUL) prediction method based on a hybrid state-space model incorporating time-varying operating conditions (TVOCs). The method features alternating parameter updates and adaptive model selection, enabling robust degradation tracking and anomaly detection under limited data scenarios. Yi et al. [14] proposed a data-driven RUL prediction method for power MOSFETs considering nonlinear dynamical behaviors. Phase space reconstruction is performed on degradation time series, and nonlinear indices are extracted to construct a novel health indicator, which is then fed into an LSTM network for prediction.

Hybrid-driven methods integrate physical models with data-driven prediction approaches for PRUL prediction of electromechanical systems, thereby combining the advantages of both prediction methods. Duan et al. [15] proposed a hybrid-driven RUL prediction method combining an asymmetric dual-channel autoencoder with a nonlinear Wiener process. The autoencoder extracts health indicators in an unsupervised manner, while the

Wiener process yields RUL probability density functions with uncertainty quantification. Wang et al. [16] developed a physics-data hybrid-driven framework for online RUL prediction of rolling bearings. By establishing synergistic mappings among defect quantification, vibration features and performance degradation, the method deeply couples bearing failure dynamics with multi-scale deep synergistic networks under monotonicity-constrained physics-informed loss.

A digital twin is an advanced form of a hybrid-driven RUL prediction approach. By integrating virtual simulation techniques with real-time monitoring technologies [17], incorporating interface technologies and data storage technologies, it forms a physical–digital fusion system, thereby providing a research framework for the real-time dynamic prediction of the PRUL of CNC rotary tables. He et al. [18] proposed a bearing remaining useful life (RUL) prediction method that employs a two-stage updated digital twin combined with a dual-correlation dynamic graph convolutional network (DC-DGCN). In this method, a bidirectional long short-term memory (Bi-LSTM) network maps vibration signals to twin defect features, thereby improving prediction accuracy by capturing the correlations between the physical and digital spaces. Cui et al. [19] proposed a digital twin-driven graph domain adaptation method for bearing RUL prediction. A full-lifecycle dynamic twin model generates abundant twin data, and a multi-layered cross-domain gated graph convolutional network with graph Laplacian regularized maximum mean discrepancy achieves effective prediction under limited actual data. Lu et al. [20,21] proposed a hybrid prediction method based on digital twin and LSTM, fusing theoretical and actual values via particle swarm optimization, and applied it to rolling bearing RUL prediction (accuracy > 97.5%) and CNC spindle thermal error prediction (accuracy improved by about 11%).

In summary, existing remaining useful life (RUL) prediction methods each have their own strengths and limitations. Model-driven methods offer strong interpretability but fail to account for random factors affecting individual units under actual operating conditions, thus lacking personalization. Data-driven methods use real-time data to reflect the actual condition of individual units; however, their prediction accuracy heavily depends on the quality and quantity of collected data, and they cannot reveal the underlying causes of performance degradation. Hybrid-driven methods combine the interpretability of theoretical models with the dynamic prediction capability of real-time data. Among these, digital twin technology provides a more systematic research framework for RUL prediction. Nevertheless, although digital twin-driven RUL prediction methods have been widely applied across various fields, existing research remains relatively limited and insufficiently in-depth when specifically targeting CNC rotary tables, thereby restricting the applicability and accuracy of this method in rotary table precision degradation prediction.

In high-precision CNC machine tools, accuracy degradation is the dominant failure mode. Therefore, it is necessary to first establish a foundation for accuracy and degradation modeling of CNC machine tools, for which Meta-action theory is a commonly used approach. Yang et al. [22] developed a kinematic and error model for multi-axis machine tools based on Meta-action theory and screw theory, and conducted simulation and experimental validation on a five-axis machining center, providing a theoretical basis for accuracy analysis of CNC machine tools. Li et al. [23] took the Meta-action unit as the basic unit, combined multi-body system topology with screw theory-based error propagation, constructed an accuracy degradation model, and realized PRUL prediction, verifying the feasibility of applying Meta-action chain error propagation to remaining useful life prediction. Louhichi and Slamani [24] systematically reviewed the Meta-action unit framework, covering multi-source error modeling, key MAU identification, PRUL prediction, and digital twin compensation, and explicitly identified five current research gaps. Through analysis of the above studies, although existing research separately addresses digital twin

modeling of thermal errors and wear degradation, a comprehensive model that integrates both within a unified digital twin framework is still lacking.

To address the above issues, this paper proposes a digital twin-driven PRUL prediction method for CNC rotary tables. This method aims to integrate the interpretability of mechanistic models with the personalization advantages of real-time data, thereby achieving accurate real-time PRUL prediction for individual CNC rotary tables. First, an overall research framework is established based on the five-dimensional digital twin model [25]. Second, starting from the analysis of precision degradation mechanisms, a theoretical model of the PRUL of CNC rotary tables is developed. Finally, a correction scheme is proposed to fuse theoretical data with real-time monitoring data to generate twin data, and a real-time PRUL prediction model for CNC rotary tables is constructed. The feasibility and effectiveness of the proposed method are verified through a case study.

2. Digital Twin Framework for Predicting Precision Remaining Useful Life of CNC Rotary Tables

According to the five-dimensional digital twin model theory [25], the digital twin framework for precision remaining useful life (PRUL) prediction of CNC rotary tables mainly consists of five components—the virtual mirror, the physical entity, the data center, the connection system, and the service system—as illustrated in Figure 1. Among them, the physical entity refers to the actual CNC rotary table in operation along with its sensing and monitoring system, which is primarily responsible for real-time data acquisition of the rotary table's precision indicators. To this end, a sensing scheme needs to be formulated to determine the sensor placement locations, signal acquisition system, and data processing methods. The virtual mirror, on the other hand, is a virtual model generated through physical modeling and mathematical modeling of the CNC rotary table. The data generated by the virtual mirror and the data acquired by the physical entity are both stored in the data center, where they are fused using appropriate methods to generate twin data, thereby providing support for subsequent services. The service system is responsible for outputting the prediction results of the digital twin framework, providing a basis for subsequent decision-making. The service executed in this paper is to utilize the twin data to achieve real-time and accurate prediction of the PRUL of the CNC rotary table. The connection system, using information transmission methods and interface protocols, enables data communication among the virtual mirror, physical entity, data center, and service system.

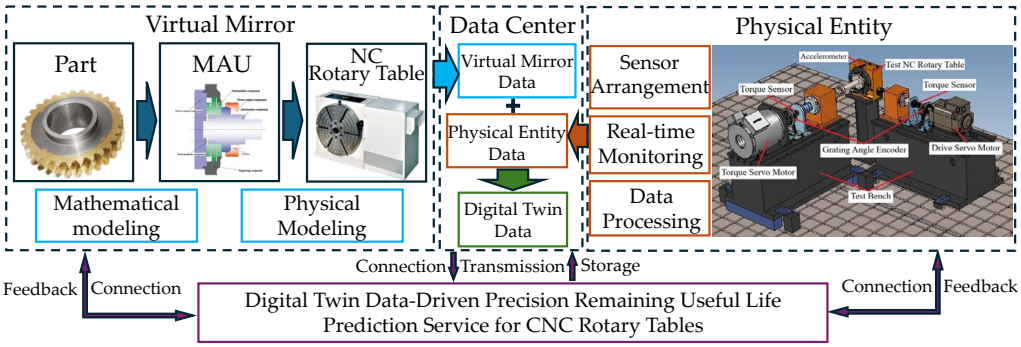


Figure 1. Structure diagram of the digital twin framework for predicting precision remaining useful life of CNC rotary tables.

It should be particularly noted that the virtual mirror characterizes the theoretical precision degradation law of the CNC rotary table by means of numerical simulation techniques and physical mechanism models. A high-fidelity virtual mirror requires that the established model cover the main influencing factors and better reflect actual operating

conditions. Therefore, when constructing the theoretical expression model for the PRUL of the CNC rotary table, the functional and kinematic essence of the rotary table must be considered. The Meta-action-based analysis method accounts for both component-level initial errors and unit-level motion errors, which is beneficial for improving the accuracy of the theoretical model. Meanwhile, empirical knowledge derived from historical data is also commonly employed in virtual mirror modeling [15].

3. Virtual Mirror Driven by Physical Models

In the virtual mirror, a theoretical expression model for the precision remaining useful life (PRUL) of the CNC rotary table needs to be established. According to the precision evolution mechanism of the CNC rotary table, the degradation of precision comprises two types of errors: first, the initial error resulting from the accumulation of manufacturing deviations in components; second, the time-varying error generated during the motion process.

3.1. Initial Precision Model Based on Error Propagation

During the manufacturing process of a CNC rotary table, machining errors of components arise due to factors such as the machining accuracy of machine tools, the skill level of operators, and uncertainties in the working environment. These errors gradually accumulate throughout the assembly process, forming the initial precision of the CNC rotary table. Therefore, it is necessary to formulate an error representation model and an error accumulation model. Prior to modeling, the following assumptions are made: all components involved in precision accumulation are considered rigid bodies; the contact surfaces during assembly are assumed to be rigid mating surfaces; and all errors are regarded as infinitesimal quantities relative to the geometric dimensions of the components. Accordingly, the specific modeling steps are as follows:

Step 1: Determination of error types. According to screw theory [22,26], the spatial pose of a component can be represented by coordinates along six degrees of freedom in a spatial coordinate system. Machining errors can be viewed as tiny offsets of the actual pose relative to the ideal pose. The mathematical expression is:

$$\boldsymbol{T} = \begin{bmatrix} 1 & -\Delta\gamma & \Delta\beta & \Delta x \\ \Delta\gamma & 1 & -\Delta\alpha & \Delta y \\ -\Delta\beta & \Delta\alpha & 1 & \Delta z \\ 0 & 0 & 0 & 1 \end{bmatrix} \tag{1}$$

where $\boldsymbol{v} = (\Delta x, \Delta y, \Delta z)^{\mathrm{T}}$ represents the infinitesimal translational displacements along the x, y and z directions, respectively, and $\boldsymbol{\theta} = (\Delta\alpha, \Delta\beta, \Delta\gamma)^{\mathrm{T}}$ represents the infinitesimal rotational displacements about the α, β, and γ axes, respectively. According to the different degrees of freedom constrained by various errors of the CNC rotary table components, these errors can be classified into planar-type errors, cylindrical-type errors, and gear-type errors. The coordinate system construction and corresponding illustrations for different error types are given in Appendix B Table A3.

Planar-type errors result from the assembly of two planar surfaces, which constrains the degrees of freedom in the x, β, and γ directions. Consequently, the planar-type error can be expressed as $\boldsymbol{T}_{\mathrm{P}}$:

$$\boldsymbol{T}_{\mathrm{P}} = \begin{bmatrix} 1 & -\Delta\gamma & \Delta\beta & \Delta x \\ \Delta\gamma & 1 & 0 & 0 \\ -\Delta\beta & 0 & 1 & 0 \\ 0 & 0 & 0 & 1 \end{bmatrix} \tag{2}$$

Cylindrical-type errors result from the shaft–hole fit, which constrains the degrees of freedom in the y, z, β, and γ directions. Consequently, the cylindrical-type error can be expressed as $\boldsymbol{T}_{\mathrm{C}}$:

$$\boldsymbol{T}_{\mathrm{C}} = \begin{bmatrix} 1 & -\Delta\gamma & \Delta\beta & 0 \\ \Delta\gamma & 1 & 0 & \Delta y \\ -\Delta\beta & 0 & 1 & \Delta z \\ 0 & 0 & 0 & 1 \end{bmatrix} \tag{3}$$

For CNC rotary tables, the gear-type errors that affect the output precision mainly include tooth thickness error and eccentricity error. Considering that both the tooth profile error and the tooth thickness error influence the tooth backlash, these two types of errors are collectively categorized as the tooth thickness error $\boldsymbol{T}_{\mathrm{T}}$ for computational convenience. It can be expressed as:

$$\boldsymbol{T}_{\mathrm{T}} = \begin{bmatrix} 1 & 0 & 0 & \Delta x \\ 0 & 1 & 0 & 0 \\ 0 & 0 & 1 & 0 \\ 0 & 0 & 0 & 1 \end{bmatrix} \tag{4}$$

The eccentricity error $\boldsymbol{T}_{\mathrm{E}}$ of the gear typically constrains the translational degrees of freedom in the x and y directions. Therefore, it can be expressed as:

$$\boldsymbol{T}_{\mathrm{E}} = \begin{bmatrix} 1 & 0 & 0 & \Delta x \\ 0 & 1 & 0 & \Delta y \\ 0 & 0 & 1 & 0 \\ 0 & 0 & 0 & 1 \end{bmatrix} \tag{5}$$

Step 2: Determine the error propagation path. The various geometric errors of components gradually accumulate along the assembly sequence, ultimately forming the output precision of the CNC rotary table. However, simply accumulating errors according to the assembly sequence alone would neglect the relative motion relationships of kinematic pairs. The Meta-action theory sorts the moving components in a mechanical system according to the motion transmission path, grouping other components rigidly connected to the moving component into one Meta-action unit, thereby achieving the separation of static and dynamic components in the mechanical system [22]. The structure and its structural decomposition results of the CNC rotary table are shown in Figure 2. It should be particularly noted that Figure 2 uses different colors to distinguish the five constituent components of a Meta-action unit. Since fasteners (e.g., screws) are standard and readily identifiable structures, they are not annotated in the figure to reduce the complexity of the structural decomposition diagram. In addition, the influence of the braking mechanism of the CNC rotary table on the output accuracy is negligible; therefore, it is also excluded from the structural decomposition. Within a Meta-action unit, attention is paid to the accumulation of geometric errors of each part according to the assembly sequence; between Meta-action units, attention is paid to the accumulation of errors according to the motion transmission sequence. This modeling approach better reflects the kinematic essence of mechanical systems [27].

Step 3: Establishment of the initial precision model of the CNC rotary table. For precision modeling within a Meta-action unit, based on the characteristic that the Meta-action focuses on the moving component, the spatial pose state of the power output component is taken as the output precision of the Meta-action unit. Let the rth type of geometric error of the power input component within the Meta-action unit be denoted as $\boldsymbol{E}_{1r}$ (r = 1, 2, …, R), the sth type of geometric errors of ith supporting components be denoted as $\boldsymbol{E}_{2is}$ (i = 1, 2, …, I; s = 1, 2, …, S), the oth type of geometric errors of jth

intermediate components be denoted as $\boldsymbol{E}_{3jo}$ ($j = 1, 2, \ldots, J$; $o = 1, 2, \ldots, O$), and the uth type of geometric error of the power output component be denoted as $\boldsymbol{E}_{4u}$ ($u = 1, 2, \ldots, U$). Then, according to the error accumulation path within the Meta-action unit, as shown in Figure 3, the output precision $\boldsymbol{E}_{\mathrm{MAU}}$ of the Meta-action unit can be calculated as:

$$\boldsymbol{E}_{\mathrm{MAU}} = \sum_{r=1}^{R} \boldsymbol{E}_{1r} + \sum_{i=1}^{I} \sum_{s=1}^{S} \boldsymbol{E}_{2is} + \sum_{j=1}^{J} \sum_{o=1}^{O} \boldsymbol{E}_{3jo} + \sum_{u=1}^{U} \boldsymbol{E}_{4u} \tag{6}$$

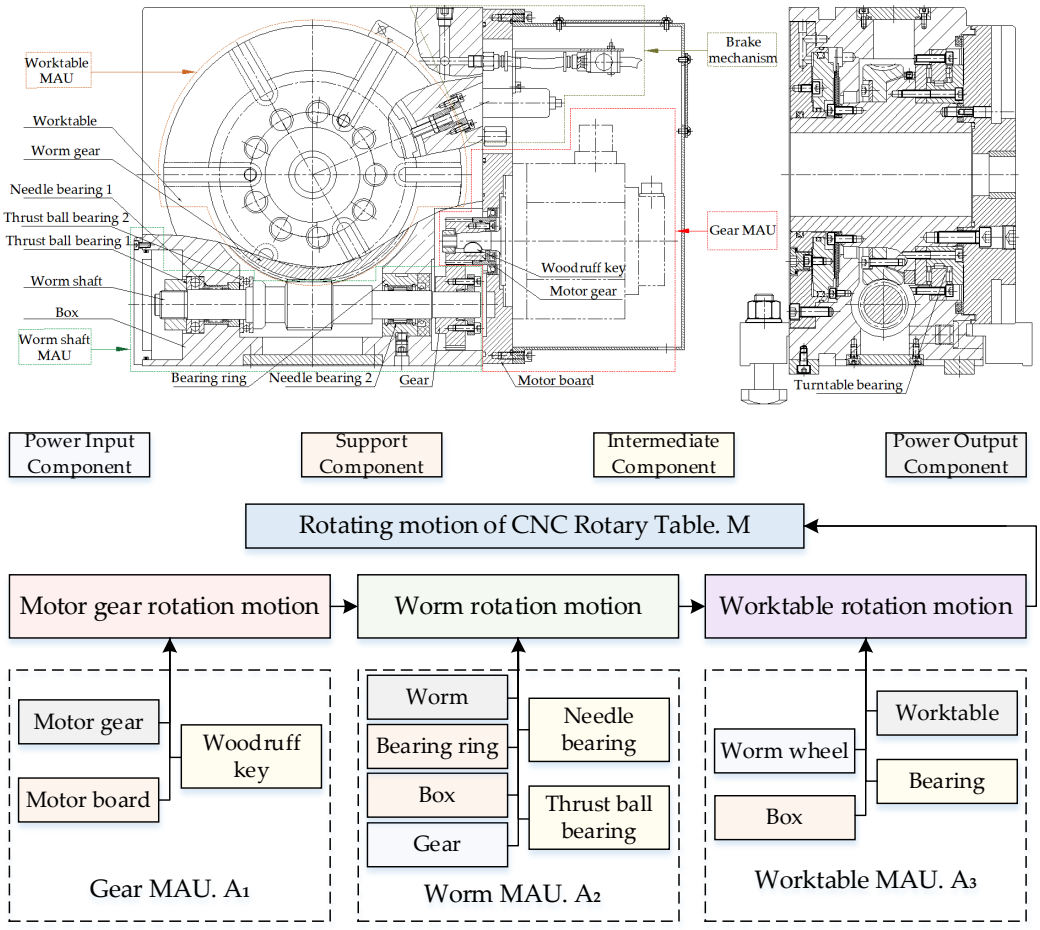


Figure 2. Structured decomposition of the CNC rotary table based on Meta-action theory.

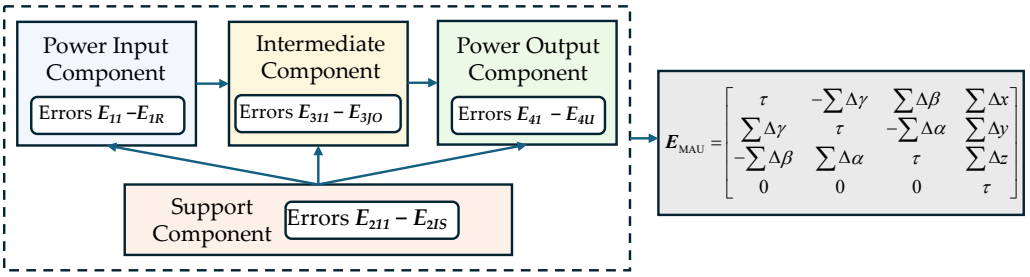


Figure 3. Error accumulation path within the Meta-action unit.

For the specific CNC rotary table investigated in this paper, the tolerance ranges and distribution parameters of the errors considered in this study for each part are listed in Appendix C Table A4. Corresponding to Appendix C Table A4, the values of the error subscripts in each Meta-action unit are shown as Table 1. For rotary tables with different structures or when different types of errors are considered, the specific values of these subscripts should be determined on a case-by-case basis.

Table 1. Values of error subscripts in each Meta-action unit.

MAU	R	I	S	J	O	U
Gear MAU	0	1	2	1	1	2
Worm MAU	3	1	2	3	Thrust ball bearing Bearing ring Needle bearing	2 3 2	4
Worktable MAU	3	1	1	2	Turntable bearing Turntable spindle	2 4	1

(It should be noted that the power input component of the Gear MAU is the motor. Its errors are not considered in this paper. Therefore, the number of error categories related to the Gear MAU's input component is zero).

For precision modeling between Meta-action units, since the output precision of a CNC rotary table involves multiple indicators—such as indexing positioning accuracy, repeat positioning accuracy, and face runout—different precision indicators represent errors in different directions within the spatial coordinate system. As the smallest motion unit in a CNC rotary table, when analyzing a specific precision indicator of the rotary table, the error component of the Meta-action unit in the corresponding direction should be taken as the output precision of that Meta-action unit. The error accumulation process between Meta-action units is illustrated in Figure 4.

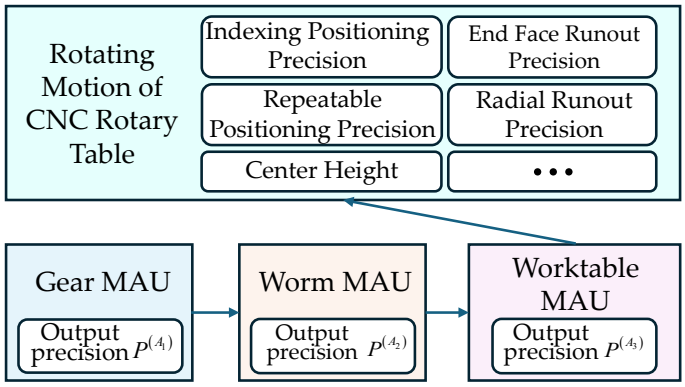


Figure 4. Error accumulation process of the inter-Mate-Action Units.

The accuracy considered in this paper for the CNC rotary table is primarily the indexing positioning accuracy, and its main influencing factor is the backlash between the gear pair and the worm gear pair. As shown by the gear-type errors in Appendix B Table A3, the output errors of the Gear MAU and the Worm MAU are both their components along the x-direction. Since the worktable of the CNC rotary table is rigidly connected to the worm wheel, the indexing positioning error of the worktable mainly depends on the motion error of the worm wheel. Considering the coordinate system arrangements for both gear-type errors (worm wheel) and cylindrical-type errors (worktable), the y-axis of the worktable part coordinate system aligns with the x-axis of the worm wheel part coordinate system. Consequently, the output error of the Worktable MAU is its component along the y-direction. Accordingly, let the output precision of the Gear MAU in the x-direction be denoted as $P_x^{(A_1)}$, the output precision of the Worm MAU in the x-direction be denoted as $P_x^{(A_2)}$, and the output precision of the Worktable MAU in the y-direction be denoted as $P_y^{(A_3)}$. Then, the initial assembly precision P_R of the CNC rotary table can be expressed as:

$$P_R = P_x^{(A_1)} + P_x^{(A_2)} + P_y^{(A_3)} \tag{7}$$

The output error of a Meta-action unit is the error accumulation of its constituent parts along the output direction. According to Appendix B Table A3, the planar-type error has three components ($\Delta\beta$, $\Delta\gamma$ and Δx), the cylindrical-type error has four components ($\Delta\beta$, $\Delta\gamma$, Δy and Δz), the tooth thickness error has one component (Δx) and the eccentricity error has two components (Δx and Δy). Since the contribution distributions of different error components to different error types are difficult to obtain, this paper assumes that the contribution degree of each error component is equal across all error types. Therefore, after taking the arithmetic mean of each type of error, the value of each error component can be obtained, and these values are identical. Based on this, according to the error types and component numbers for each part in each Meta-action unit listed in Appendix C Table A4, the distribution data of $P_x^{(A_1)}$, $P_x^{(A_2)}$, and $P_y^{(A_3)}$ can be calculated as follows:

$$\begin{cases} \mu_x^{(A_1)} = \sum\limits_{r=1}^{R} \frac{\mu_{1r}^{(A_1)}}{n_{1r}^{(A_1)}} + \sum\limits_{i=1}^{I}\sum\limits_{s=1}^{S} \frac{\mu_{2is}^{(A_1)}}{n_{2is}^{(A_1)}} + \sum\limits_{j=1}^{J}\sum\limits_{o=1}^{O} \frac{\mu_{3jo}^{(A_1)}}{n_{3jo}^{(A_1)}} + \sum\limits_{u=1}^{U} \frac{\mu_{4u}^{(A_1)}}{n_{4u}^{(A_1)}} \\ \sigma_x^{(A_1)} = \sqrt{\sum\limits_{r=1}^{R} \left(\frac{\sigma_{1r}^{(A_1)}}{n_{1r}^{(A_1)}}\right)^2 + \sum\limits_{i=1}^{I}\sum\limits_{s=1}^{S} \left(\frac{\sigma_{2is}^{(A_1)}}{n_{2is}^{(A_1)}}\right)^2 + \sum\limits_{j=1}^{J}\sum\limits_{o=1}^{O} \left(\frac{\sigma_{3jo}^{(A_1)}}{n_{3jo}^{(A_1)}}\right)^2 + \sum\limits_{u=1}^{U} \left(\frac{\sigma_{4u}^{(A_1)}}{n_{4u}^{(A_1)}}\right)^2} \\ \mu_x^{(A_2)} = \sum\limits_{r=1}^{R} \frac{\mu_{1r}^{(A_2)}}{n_{1r}^{(A_2)}} + \sum\limits_{i=1}^{I}\sum\limits_{s=1}^{S} \frac{\mu_{2is}^{(A_2)}}{n_{2is}^{(A_2)}} + \sum\limits_{j=1}^{J}\sum\limits_{o=1}^{O} \frac{\mu_{3jo}^{(A_2)}}{n_{3jo}^{(A_2)}} + \sum\limits_{u=1}^{U} \frac{\mu_{4u}^{(A_2)}}{n_{4u}^{(A_2)}} \\ \sigma_x^{(A_2)} = \sqrt{\sum\limits_{r=1}^{R} \left(\frac{\sigma_{1r}^{(A_2)}}{n_{1r}^{(A_2)}}\right)^2 + \sum\limits_{i=1}^{I}\sum\limits_{s=1}^{S} \left(\frac{\sigma_{2is}^{(A_2)}}{n_{2is}^{(A_2)}}\right)^2 + \sum\limits_{j=1}^{J}\sum\limits_{o=1}^{O} \left(\frac{\sigma_{3jo}^{(A_2)}}{n_{3jo}^{(A_2)}}\right)^2 + \sum\limits_{u=1}^{U} \left(\frac{\sigma_{4u}^{(A_2)}}{n_{4u}^{(A_2)}}\right)^2} \\ \mu_x^{(A_3)} = \sum\limits_{r=1}^{R} \frac{\mu_{1r}^{(A_3)}}{n_{1r}^{(A_3)}} + \sum\limits_{i=1}^{I}\sum\limits_{s=1}^{S} \frac{\mu_{2is}^{(A_3)}}{n_{2is}^{(A_3)}} + \sum\limits_{j=1}^{J}\sum\limits_{o=1}^{O} \frac{\mu_{3jo}^{(A_3)}}{n_{3jo}^{(A_3)}} + \sum\limits_{u=1}^{U} \frac{\mu_{4u}^{(A_3)}}{n_{4u}^{(A_3)}} \\ \sigma_x^{(A_3)} = \sqrt{\sum\limits_{r=1}^{R} \left(\frac{\sigma_{1r}^{(A_3)}}{n_{1r}^{(A_3)}}\right)^2 + \sum\limits_{i=1}^{I}\sum\limits_{s=1}^{S} \left(\frac{\sigma_{2is}^{(A_3)}}{n_{2is}^{(A_3)}}\right)^2 + \sum\limits_{j=1}^{J}\sum\limits_{o=1}^{O} \left(\frac{\sigma_{3jo}^{(A_3)}}{n_{3jo}^{(A_3)}}\right)^2 + \sum\limits_{u=1}^{U} \left(\frac{\sigma_{4u}^{(A_3)}}{n_{4u}^{(A_3)}}\right)^2} \end{cases} \tag{8}$$

where n is the component number for the corresponding error type, which can be found in Appendix C Table A4.

Therefore, the distribution of the initial assembly accuracy P_R of the CNC rotary table can be calculated as follows:

$$\begin{cases} \mu_R = \mu_x^{(A_1)} + \mu_x^{(A_2)} + \mu_y^{(A_3)} \\ \sigma_R = \sqrt{\left(\sigma_x^{(A_1)}\right)^2 + \left(\sigma_x^{(A_2)}\right)^2 + \left(\sigma_x^{(A_3)}\right)^2} \end{cases} \tag{9}$$

3.2. Mathematical Expression Model for Time-Varying Errors

Due to the characteristics of substantial heat generation and susceptibility to wear inherent in worm gear drives, thermal error and wear error constitute the primary error sources affecting the precision life of CNC rotary tables. Therefore, it is necessary to perform theoretical modeling of these two types of errors from the perspective of numerical analysis.

3.2.1. Thermal Error Simulation

Thermal error generally requires solving via the finite element method to obtain the thermal deformation of components within a steady-state temperature field. Considering that frictional heat is typically concentrated on the contacting tooth surfaces where relative motion occurs, and has a relatively minor effect on other fixedly connected components

within the Meta-action unit, for ease of solution, the thermal error primarily considers the thermal deformation of the worm wheel and the worm.

It should be noted that the thermal error simulation is subject to three assumptions: (1) the mechanical structure is treated as a continuous, isotropic medium; (2) upon reaching thermal equilibrium, the temperature field is steady and uniformly distributed; and (3) the thermal conductivity, specific heat capacity, linear expansion coefficient, and elastic modulus are all taken as constant values throughout the simulation.

The specific simulation steps are as follows:

Step 1: Denote the temperature field of the worm gear pair in the Cartesian coordinate system as $T = T(x,y,z,t)$. Under steady-state conditions, after a period of heat exchange, the heat Q inside the worm gear pair and on its boundaries results in a stable temperature at each point of the components, i.e.,

$$\frac{\partial T}{\partial t} = 0 \tag{10}$$

Therefore, given the temperature field $T = T(x,y,z,t)$, the three-dimensional steady-state heat conduction model can be expressed as:

$$\rho c \frac{\partial T}{\partial t} = \frac{\partial}{x}\left(\lambda_x \frac{\partial T}{\partial x}\right) + \frac{\partial}{y}\left(\lambda_y \frac{\partial T}{\partial y}\right) + \frac{\partial}{z}\left(\lambda_z \frac{\partial T}{\partial z}\right) + \phi \tag{11}$$

where λ_x, λ_y, λ_z is the thermal conductivity coefficient of the material in each direction; ϕ is the internal heat source; ρ is the density of the material; c is the specific heat capacity.

Step 2: The internal heat source of the worm gear pair is primarily the heat generated by friction. Therefore, the formula for the instantaneous frictional heat flux per unit area on the contact surface of the worm gear pair, denoted as q_{m}, is:

$$q_{\mathrm{m}} = fpv_{\mathrm{s}} \tag{12}$$

where f is the friction coefficient of the worm gear pair; p is the contact stress; v_{s} is the relative sliding velocity.

Step 3: Determine the boundary conditions on each surface of the worm gear pair. The tooth meshing zone is subjected to both frictional heat flux and convective thermal boundary conditions, simultaneously satisfying the Neumann boundary condition and the third kind of boundary condition. The boundary conditions can be expressed as:

$$-\lambda\left(\frac{\partial T}{\partial n}\right) = h_{\mathrm{m}}(T - T_{\mathrm{m}}) + q_{\mathrm{m}} \tag{13}$$

where $\frac{\partial T}{\partial n}$ is the temperature gradient; h_{m} is the convective heat transfer coefficient of the tooth meshing zone; T_{m} is the medium temperature for convective heat transfer in the tooth meshing zone.

The tooth tip surface, tooth root surface, non-working areas of the meshing surface, and the end faces of the worm wheel are all subject solely to convective heat transfer boundary conditions, which satisfy the third kind of boundary condition. The boundary conditions can be expressed as:

$$-\lambda\left(\frac{\partial T}{\partial n}\right) = h_{\mathrm{s}}(T - T_{\mathrm{s}}) \tag{14}$$

where h_{s} is the convective heat transfer coefficient of the non-working area; T_{s} is the medium temperature for convective heat transfer in the non-working area.

The bottom surface of the worm wheel is located far from the meshing zone and can therefore be assumed to be an adiabatic surface. The boundary condition is:

$$\frac{\partial T}{\partial n} = 0 \tag{15}$$

Step 4: According to the empirical formula, the heat partition coefficient β between the worm and the worm wheel is given by:

$$\beta = \frac{\sqrt{\lambda_1 \rho_1 c_1 v_{1t}}}{\sqrt{\lambda_1 \rho_1 c_1 v_{1t}} + \sqrt{\lambda_2 \rho_2 c_2 v_{2t}}} \tag{16}$$

where λ_1 and λ_2 are the thermal conductivities of the worm wheel and worm materials, respectively; ρ_1 and ρ_2 are the densities of the worm wheel and worm materials, respectively; c_1 and c_2 are the specific heat capacities of the worm wheel and worm materials, respectively; v_{1t} and v_{2t} are the relative tangential velocities of the worm wheel and worm at the meshing point, respectively.

Step 5: Establish a finite element model of the worm gear pair, assign the material properties of the components, perform mesh generation, apply boundary conditions such as heat flux and convective heat transfer coefficients, and solve for the thermal strain results e_{hw} and e_{hg} of the worm wheel and the worm under the steady-state temperature field.

3.2.2. Wear Error Modeling

The wear errors in CNC rotary tables primarily stem from the wear of the worm wheel and the wear of the rotary table bearing. Since the worm wheel is typically made of copper alloy while the worm is usually made of alloy steel, this material combination leads to a significantly higher wear rate of the worm wheel, which is generally much greater than that of the worm and gears. The rotary table bearing, due to its substantial load-bearing requirements, exhibits a wear rate far exceeding that of other bearings. Therefore, this paper employs the Archard wear model to calculate the wear errors of the worm wheel and the bearing. By discretizing the wear process, the wear amount at each infinitesimal time step is obtained as:

$$\Delta h(t) = \int_0^{\Delta t} k p v_s \mathrm{d}t \tag{17}$$

where k is the wear coefficient of the material; p is the contact stress in the contact zone; v_s is the relative motion velocity of the contact surface.

The infinitesimal time interval Δt for each contact can be calculated as:

$$\Delta t = \frac{q}{v_s} \tag{18}$$

where q is the half-width of the Hertz contact zone, which can be calculated according to the Hertz contact equations.

For the worm wheel, the relative motion velocity v_{ws} can be calculated as:

$$v_{ws} = \frac{v_1}{\cos\gamma} = \frac{\pi d_1 n_1}{60 \times 1000 \cos\gamma} \tag{19}$$

where d_1 is the pitch diameter of the worm; n_1 is the rotational speed of the worm; γ is the lead angle.

The contact stress between the worm and the worm wheel can be calculated as:

$$p_w = 480\sqrt{\frac{KT_2}{d_1 m^2 Z_2^2}} \tag{20}$$

where, since the worm wheel rotary table typically operates under a stable load, the load factor $K = 1$; T_2 is the torque of the worm wheel; m is the module of the worm; Z_2 is the number of teeth of the worm wheel.

Let the rotational speed of the CNC rotary table be $\widetilde{n}$, the operating time be t, and the wear amount at each contact instant be Δh_w. Then the total wear amount on the tooth surface of the worm wheel can be calculated as:

$$e_{ww}(t) = \Delta h_w \cdot \widetilde{n} \cdot t \tag{21}$$

For the rotary table bearing, the main wear locations are the outer raceway, the inner raceway, and the rollers. The forces acting on the rollers are shown in Figure 5. Considering that the output rotational speed of the rotary table is relatively low, the centrifugal force F_C can be neglected. The pressure N_1 on the inner raceway and the supporting force N_2 on the outer raceway are determined by the weight of the worktable and the load. f_1 and f_2 are the frictional forces, while F_k^1 and F_k^2 are the forces exerted by the cage on the rollers. Accordingly, the contact stress between the rollers and the raceways can be calculated as:

$$p_g = \frac{N_2}{q_g} \tag{22}$$

where q_g is the half-width of the Hertz contact zone.

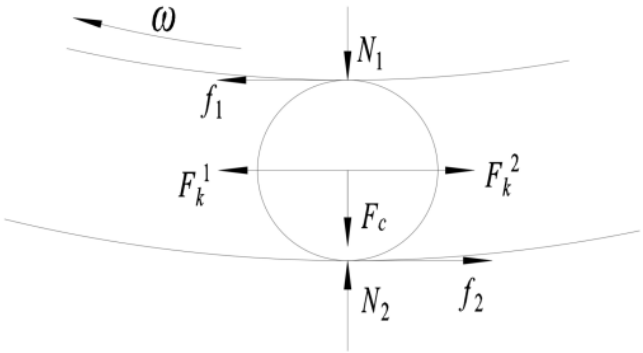


Figure 5. Force Analysis of the Roller.

The rotational speed of the inner ring of the rotary table bearing is equal to the rotational speed $\widetilde{n}$ of the rotary table. Let the contact circle diameter of the inner raceway be R_1. Then the relative motion velocity v_{gs} between the roller and the raceway can be calculated as:

$$v_{gs} = \frac{\pi R_1 \widetilde{n}}{60} \tag{23}$$

The wear amount $e_{gw}(t)$ of the rotary table bearing can be calculated as:

$$e_{gw}(t) = \Delta h_1 \cdot \widetilde{n} \cdot z \cdot t + \Delta h_2 \cdot \frac{2R_1}{R_0} \cdot \widetilde{n} \cdot t + \Delta h_3 \cdot \widetilde{n} \cdot z \cdot t \tag{24}$$

where R_0 is the diameter of the roller, z is the number of rollers, and Δh_1, Δh_2 and Δh_3 are the wear amounts per contact of the inner raceway, the roller, and the outer raceway, respectively, calculated by Equation (17).

3.3. Theoretical Model of Precision Remaining Useful Life

The accumulation of errors during the manufacturing process of a CNC rotary table forms its initial output precision, while time-varying errors such as component wear and aging during operation cause the degradation of the output precision. In addition, the

CNC rotary table is also subject to various environmental factors under actual working conditions, leading to uncertainty in the output precision. This results in a phenomenon of fluctuated degradation in the actual output precision of the CNC rotary table. The Wiener process model is well suited for the quantitative characterization of such stochastic degradation processes [28]. Let $X(t);t \geq 0$ denote the output precision. Then the Wiener process model can be expressed as:

$$X(t) = x_0 + \mu t + \sigma_B B(t) \tag{25}$$

where x_0 is the initial output precision of the CNC rotary table, which can be solved using the models in Sections 3.1 and 3.2; μ is the drift coefficient related to the degradation rate, which can be obtained from the wear amount calculation model in Section 3.2; σ_B is the diffusion coefficient associated with the degree of uncertainty; $B(t)$ is the standard Brownian motion. Since the uncertainty of the operating process is difficult to quantify theoretically using a physical model, it can be fitted using historical data from similar products.

Let the precision threshold of the CNC rotary table be denoted as ξ. Then the precision life of the CNC rotary table can be defined as the time when the output precision first reaches the precision threshold, expressed as:

$$T = \inf\{t{:}X(t) \geq \xi \mid X(0) < \xi)\} \tag{26}$$

And the time duration from any given time t_i until the output precision first reaches the precision threshold is the precision remaining useful life of the CNC rotary table at time t_i, denoted as:

$$T_{\mathrm{RUL}} = \inf\{t : X(t + t_i) \geq \xi \mid X(t_i) < \xi)\} \tag{27}$$

According to the properties of the Wiener process model, the precision remaining useful life T_{RUL} follows an inverse Gaussian distribution. Let the output precision of the rotary table at any arbitrary time t_i be x_{t_i}. Therefore, the distribution function of the precision remaining useful life of the CNC rotary table at time t_i can be expressed as:

$$F_T(t) = \Phi\left(\frac{x_{t_i} + \mu t - \xi}{\sigma_B\sqrt{t}}\right) + \exp\left(\frac{2\mu(\xi - x_{t_i})}{\sigma_B^2}\right)\Phi\left(\frac{-(\xi - x_{t_i}) - \mu t}{\sigma_B\sqrt{t}}\right) \tag{28}$$

The probability density function of the precision remaining useful life of the CNC rotary table at time t_i can be expressed as:

$$f_T(t) = \frac{\xi - x_{t_i}}{\sigma_B\sqrt{2\pi t^3}}\exp\left(-\frac{(\xi - x_{t_i} - \mu t)^2}{2\sigma_B^2 t}\right) \tag{29}$$

4. Monitoring Data-Driven Physical Entity

Real-time monitoring data are characteristic quantities that reflect the actual operating state of a CNC rotary table, acquired through sensor technology and signal acquisition techniques. They can truthfully represent the precision life status of the CNC rotary table. However, the accuracy of these data depends on the precision of the sensors and the interference from environmental noise. Therefore, when designing the monitoring scheme, several factors need to be considered: the sensor arrangement should not interfere with the normal operation of the rotary table; the number of interference points in the acquisition process should be minimized; the acquired precision indicators should directly or indirectly reflect the precision status of the CNC rotary table; and the sampling interval should not be excessively large so as to capture the fluctuations of the precision indicators. In this study, a precision life test bench for CNC rotary tables was employed to simulate the working

state under actual load conditions and to acquire real-time precision monitoring data. As shown in Figure 6, the test bench consists of five components: the CNC rotary table body, the drive motor, the load motor, the sensing system, and the supporting base. The sensors used are two angular encoders installed at the driving end and the loading end, whose performance specifications are listed in Table 2. The difference between the readings of the two encoders constitutes the indexing positioning accuracy of the CNC rotary table. Test conditions were set according to typical working loads, output rotational speeds, and output torques, and the real-time monitoring data were recorded and stored.

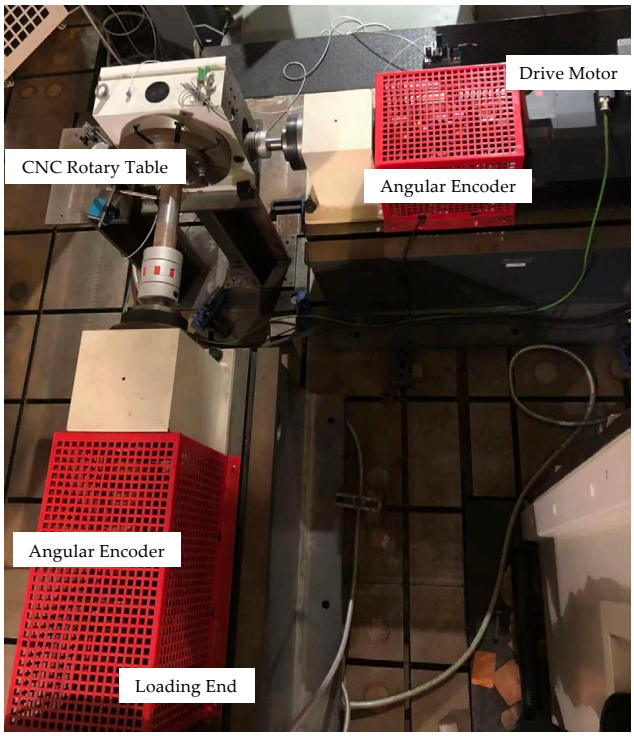


Figure 6. Precision life test bench of CNC rotary table.

Table 2. Main performance index of grating angle encoder.

Item	Model	Lines per Revolution	Overall Accuracy	Maximum Allowable Speed (r/min)	Shaft Diameter (mm)
Driving End	HEIDENHAIN ERA4482C	6000 lines	$\pm 5''$	$\leq$1000	40
Loading End	HEIDENHAIN RON786	36,000 lines	$\pm 2''$	$\leq$1000	60

5. Digital Twin Data-Driven PRUL Prediction Service for CNC Rotary Tables

The theoretical simulation data obtained from the virtual mirror reflect the general pattern of precision life variation common to a class of CNC rotary tables, but they are unable to quantitatively express the random disturbances occurring during the operation of an individual rotary table. On the other hand, the quality of monitoring data acquired from the physical entity depends on the accuracy of the sensors and the duration of data acquisition, which may reduce the credibility of the prediction results. Therefore, the twin data generated by combining theoretical data with real-time data can integrate general laws with real-time characteristics, thereby not only reflecting the real-time stochastic state of the CNC rotary table but also enhancing the interpretability of the prediction results. According to the Wiener process model, three parameters need to be determined: the initial value, the drift coefficient, and the diffusion coefficient. Accordingly, the digital twin

data-driven service for predicting the precision remaining useful life of CNC rotary tables primarily focuses on correcting these three parameters, thereby achieving both accuracy and real-time capability in the prediction results.

First, the initial precision value of the CNC rotary table calculated in the virtual mirror is taken as the sum of the mean value of the normal distribution and the steady-state thermal error. However, the initial precision varies from one rotary table to another. Moreover, considering that a certain period of time is required for the CNC rotary table to reach thermal equilibrium from startup, the precision data during this period primarily exhibit random fluctuations, and such random factors only appear in the early stage of operation. Therefore, to mitigate the influence of random factors in the initial stage, the minimum value of the output error after a period of operation in the real-time data is taken as the initial precision value x_{0d} of the CNC rotary table, and the data prior to this minimum value are discarded when calculating the drift coefficient and the diffusion coefficient.

Second, let the real-time monitoring data acquired from the physical entity be denoted as (x_i,t_i), $i = 1, 2, \ldots n$. The drift coefficient μ_{p} is then fitted using linear regression as:

$$\mu_{\mathrm{p}} = \frac{\sum_{i=1}^{n}(x_i-\bar{x})\left(t_i-\bar{t}\right)}{\sum_{i=1}^{n}(x_i-\bar{x})^2 \cdot \sum_{i=1}^{n}\left(t_i-\bar{t}\right)^2} \tag{30}$$

where $\bar{x}$ is the mean value of the precision data and $\bar{t}$ is the mean value of the time data.

Let the drift coefficient calculated from the virtual simulation be denoted as μ_{v}. Then the corrected drift coefficient μ_{d} can be calculated as:

$$\mu_{\mathrm{d}} = \frac{\mu_{\mathrm{p}} + \mu_{\mathrm{v}}}{2} \tag{31}$$

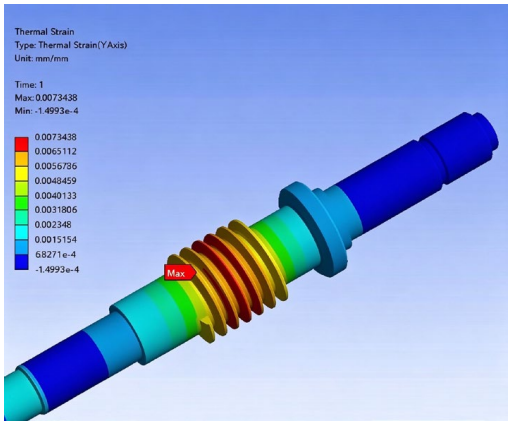
Thirdly, let the diffusion coefficient obtained by substituting the real-time monitoring data into the Wiener process model be denoted as σ_{Bp}, and the diffusion coefficient obtained by substituting historical data from similar products into the model be denoted as σ_{Bv}. Then the corrected diffusion coefficient σ_{Bd} can be calculated as:

$$\sigma_{\mathrm{Bd}}^2 = \left(\frac{\sigma_{\mathrm{Bp}}}{2}\right)^2 + \left(\frac{\sigma_{\mathrm{Bv}}}{2}\right)^2 \tag{32}$$

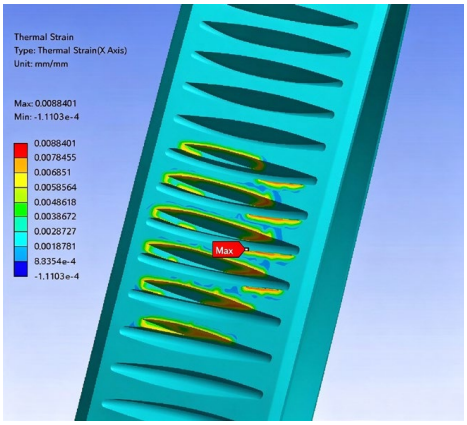
Finally, by substituting the three corrected parameters into Equation (29), the predicted values of the precision remaining useful life of the CNC rotary table at different time instants under the digital twin data-driven framework are obtained, thereby providing a basis for subsequent operation and maintenance decision-making.

6. Case Study

This paper presents a case study on the TK13 series CNC rotary table manufactured by a domestic machine tool accessory enterprise. The output precision indicator is the indexing positioning accuracy, and the precision threshold is set to ξ = 40 μm. Based on the error types and distributions in Appendix C Table A4 combined with Equations (1)–(9), the initial assembly precision of the CNC rotary table is calculated as $P_R \sim N(4.5,32.01)$. Based on Section 3.2, the thermal error simulation is performed, and the results are shown in Figure 7.



(**a**) Thermal error simulation result of worm



(**b**) Thermal error simulation result of worm wheel

Figure 7. Thermal error simulation result of the worm gear pair.

The thermal deformation of the worm under the steady-state temperature field is 7.3438 μm, and that of the worm wheel is 8.8401 μm. Consequently, the theoretical initial precision value of the CNC rotary table obtained from the virtual mirror is:

$$x_{0v} = 4.5 + 7.3438 + 8.8401 = 20.684\ \mu m \tag{33}$$

The worm gear pair uses extreme pressure gear oil for lubrication, with a lubricant pressure–viscosity coefficient of 1.6819×10^{-8} m^2/N. The surface roughness of the worm is 1.6 μm, and that of the worm wheel is 0.4 μm. The friction coefficient of the worm gear pair is 0.145. Based on the Janakiraman regression formula from reference [29], the wear coefficient k is calculated to be 7.6939×10^{-6} μm^2/N. By substituting the material parameters of the worm gear pair from Reference [30], the material parameters of the rotary table bearing from Reference [31], and the data from Appendix D Tables A5–A7 into Equations (17)–(24), the theoretical drift coefficient μ_v = 0.033 μm/h derived from the virtual mirror can be calculated. The theoretical diffusion coefficient $\sigma_{Bv}^2 = 0.1718$ is obtained by substituting the historical data of similar products from Reference [32] into the Wiener process model. Subsequently, by substituting the three calculated parameters x_{0v}, μ_v, and σ_{Bv} into Equation (29), the probability density functions of the precision remaining useful life of the CNC rotary table at 0 h, 100 h, 200 h, 300 h, and 400 h under the virtual mirror data-driven framework are solved and obtained, as shown in Figure 8.

Based on the CNC rotary table precision life test bench and the experimental scheme described in Section 4, experiments were carried out. Due to the slow precision degradation rate of the CNC rotary table, and considering the resolution of the angular encoders, the indexing positioning accuracy data were recorded at intervals of 15 h. Given that the output precision in the Wiener process model is a distance value, the angular data collected by the angular encoders were converted into arc length data. Thus, the monitoring data obtained over 450 h are listed in Table 3.

Monitoring data from 0 h to 180 h were selected for analysis. The actual initial precision value x_{0p} = 26.703 μm of the CNC rotary table was determined. The real-time drift coefficient μ_p = 0.0198 μm/h was calculated according to Equation (30). By substituting the data into the Wiener process model, the real-time diffusion coefficient $\sigma_{Bp}^2 = 0.0598$ was obtained. Substituting these three parameters into Equation (29), the probability density functions of the precision remaining useful life of the CNC rotary table at 0 h, 100 h, 200 h, 300 h, and 400 h under the monitoring data-driven framework from 0 h to 180 h were solved and obtained, as shown in Figure 9.

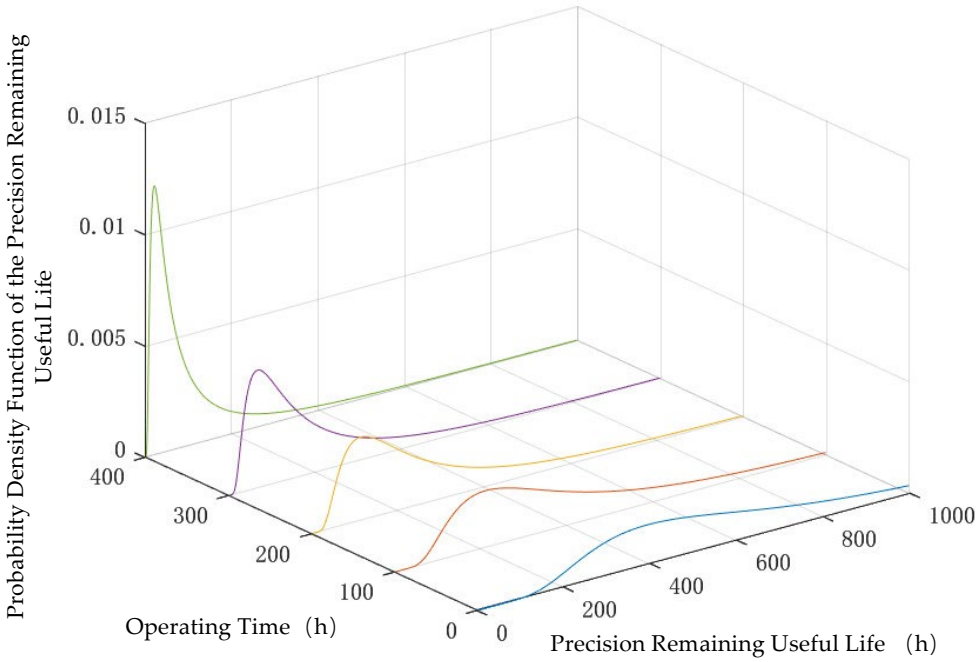


Figure 8. Predicted results of precision remaining useful life of the CNC rotary table at different time instants under the virtual mirror data-driven framework.

Table 3. Real-time data from physical entity.

Time (h)	Indexing Positioning Accuracy (μm)	Time (h)	Indexing Positioning Accuracy (μm)
15	28.274	240	34.557
30	28.274	255	34.557
45	26.703	270	32.986
60	26.703	285	34.557
75	26.703	300	34.557
90	26.703	315	32.986
105	28.274	330	34.557
120	28.274	345	36.127
135	28.274	360	37.698
150	29.844	375	37.698
165	29.844	390	39.269
180	31.415	405	37.698
195	31.415	420	39.269
210	32.986	435	42.410
225	32.986	450	42.410

Subsequently, by combining the virtual simulation data with the monitoring data from 0 h to 180 h, the precision initial value x_{0d} = 26.703 μm of the CNC rotary table under the twin data-driven framework is obtained. The corrected drift coefficient μ_d = 0.026391 μm/h is obtained according to Equation (31), and the corrected diffusion coefficient $\sigma_{Bd}^2 = 0.0579$ is obtained according to Equation (32). Substituting these three parameters into Equation (29), the probability density functions of the precision remaining useful life of the CNC rotary table at 0 h, 100 h, 200 h, 300 h, and 400 h under the twin data-driven framework from 0 h to 180 h are solved and obtained, as shown in Figure 10.

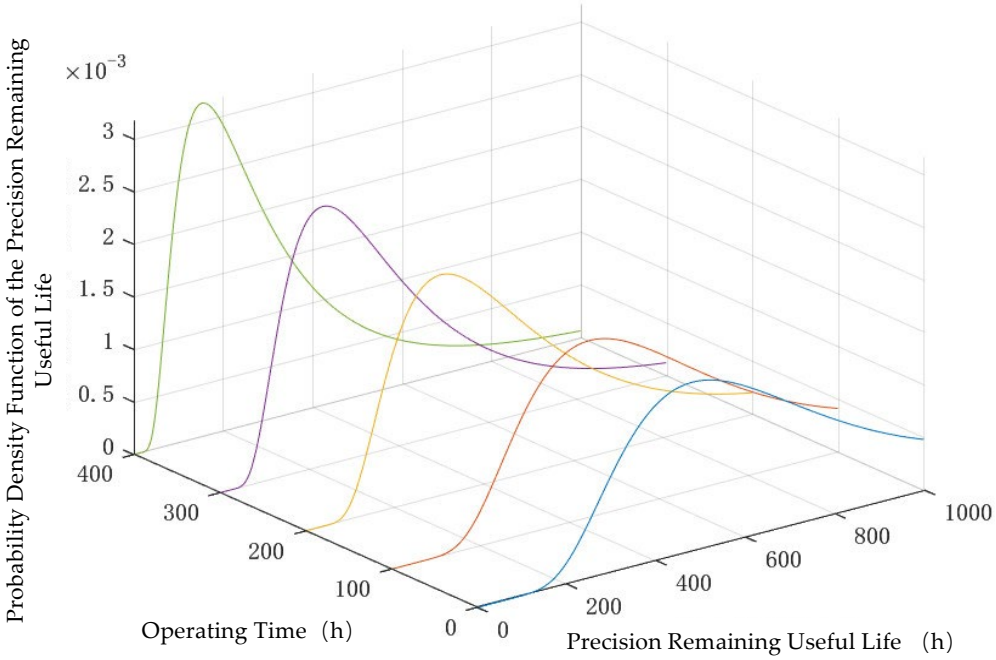


Figure 9. Predicted results of precision remaining useful life of the CNC rotary table at different time instants under the 0–180 h monitoring data-driven framework.

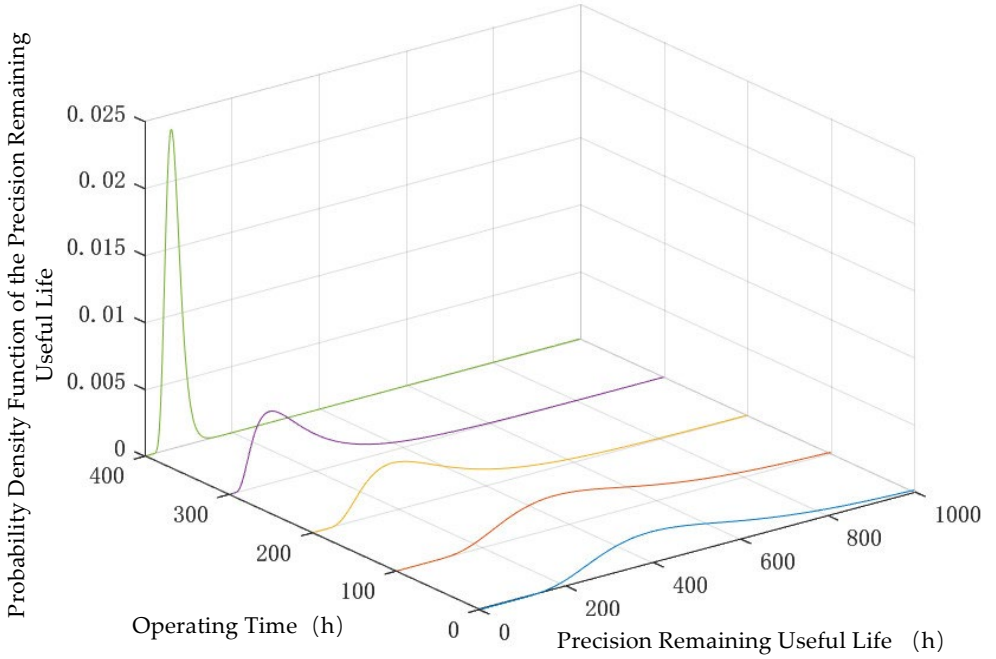


Figure 10. Predicted results of precision remaining useful life of the CNC rotary table at different time instants under the 0–180 h twin data-driven framework.

The comparison of predicted precision remaining useful life of the CNC rotary table at 0 h, 100 h, 200 h, 300 h, and 400 h under different data-driven frameworks from 0 h to 180 h, obtained from Figures 8–10, is summarized in Table 4. The comparison results indicate that, due to the small volume of monitoring data from 0 h to 180 h, the prediction based solely on monitoring data exhibits a relatively large deviation. For example, the monitoring data-driven prediction yields a precision remaining useful life of 302 h when the rotary table has operated for 200 h, which is far greater than the actual value of 235 h, and a precision remaining useful life of 152 h when the rotary table has operated for 400 h, which differs significantly from the actual value of 35 h. In contrast, the twin data can

improve prediction accuracy to a certain extent. Moreover, compared with the prediction driven solely by virtual mirror data, the integration of real-time data enables the predicted results at most time points—such as 200 h and 300 h—to be closer to the true values.

Table 4. Comparison of predicted PRUL values of the CNC rotary table at different time instants under various data-driven frameworks from 0 to 180 h.

Time (h)	0 h	100 h	200 h	300 h	400 h
Predicted Value Based on Virtual Mirror Data (h)	394	214	116	68	22
Predicted Value Based on 0–180 h Monitoring Data (h)	480	444	302	230	152
Predicted Value Based on 0–180 h Twin Data (h)	394	366	184	94	60
Actual Value (h)	435	335	235	135	35

Furthermore, monitoring data from 0 h to 360 h were selected for analysis. The actual initial precision value x_{0p} = 26.703 μm of the CNC rotary table was determined. The real-time drift coefficient μ_p = 0.0300 μm/h was calculated according to Equation (30). By substituting the data into the Wiener process model, the real-time diffusion coefficient $\sigma_{Bp}^2 = 0.0858$ was obtained. Substituting these three parameters into Equation (29), the probability density functions of the precision remaining useful life of the CNC rotary table at 0 h, 100 h, 200 h, 300 h, and 400 h under the 0 h to 360 h monitoring data-driven framework were solved and obtained, as shown in Figure 11.

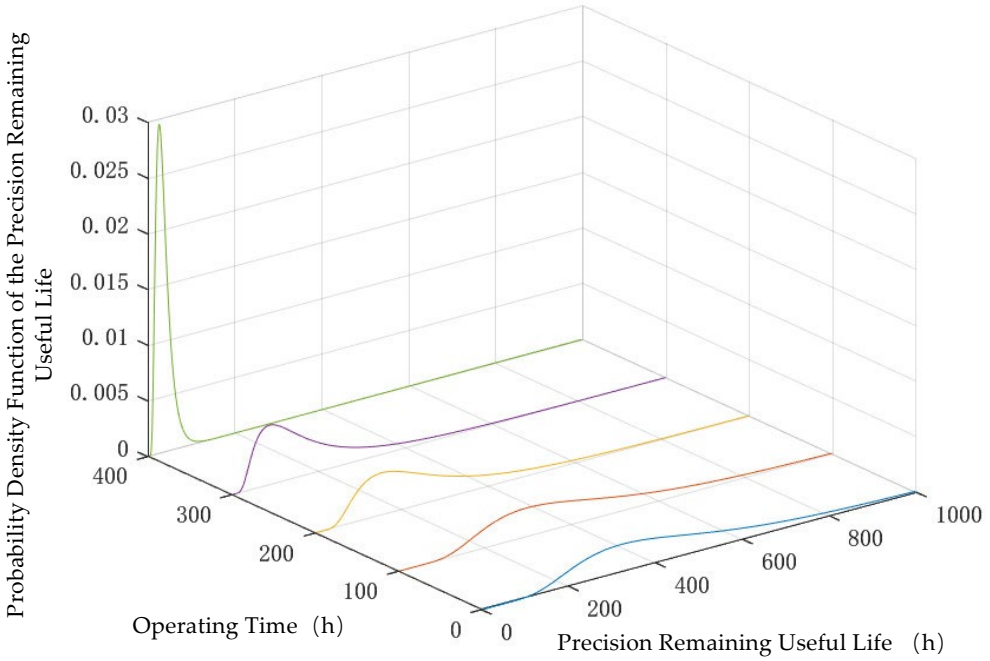


Figure 11. Predicted results of precision remaining useful life of the CNC rotary table at different time instants under the 0–360 h monitoring data-driven framework.

Subsequently, by combining the virtual simulation data with the monitoring data from 0 h to 360 h, the initial precision value x_{0d} = 26.703 μm of the CNC rotary table under the digital twin data-driven framework is obtained. The corrected drift coefficient μ_d = 0.031491 μm/h is obtained according to Equation (31), and the corrected diffusion coefficient $\sigma_{Bd}^2 = 0.0644$ is obtained according to Equation (32). Substituting these three parameters into Equation (29), the probability density functions of the precision remaining useful life of the CNC rotary table at 0 h, 100 h, 200 h, 300 h, and 400 h under the 0 h to 360 h digital twin data-driven framework are solved and obtained, as shown in Figure 12.

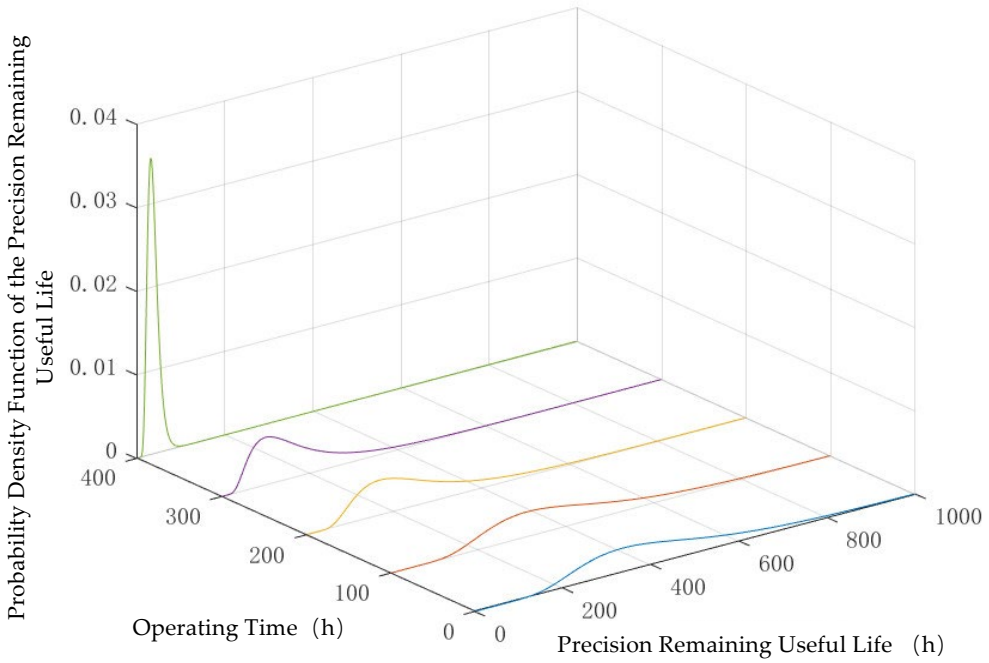


Figure 12. Predicted results of precision remaining useful life of the CNC rotary table at different time instants under the 0–360 h twin data-driven framework.

The comparison of predicted precision remaining useful life values of the CNC rotary table at 0 h, 100 h, 200 h, 300 h, and 400 h under different data-driven frameworks from 0 h to 360 h, obtained from Figures 10 and 11, is summarized in Table 5. According to the twin data-driven prediction, the precision remaining useful life is 32 h when the rotary table has operated for 400 h. Compared with the predicted value of 22 h from the virtual mirror data and the predicted value of 26 h from the monitoring data, the twin data-driven result is closer to the actual value of 35 h. This demonstrates that the precision remaining useful life prediction results driven by digital twin data are significantly superior to those driven solely by virtual mirror data or solely by monitoring data, thereby validating the effectiveness of the proposed method.

Table 5. Comparison of predicted PRUL values of the CNC rotary table at different time instants under various data-driven frameworks from 0 to 360 h.

Time (h)	0 h	100 h	200 h	300 h	400 h
Predicted Value Based on Virtual Mirror Data (h)	394	214	116	68	22
Predicted Value Based on 0–360 h Monitoring Data (h)	322	298	154	88	26
Predicted Value Based on 0–360 h Twin Data (h)	336	312	168	100	32
Actual Value (h)	435	335	235	135	35

In summary, combining the prediction results shown in Tables 4 and 5, the Mean Absolute Error (MAE) and Root Mean Square Error (RMSE) of the three prediction methods are calculated, as shown in Table 6.

Taking the prediction errors based on twin data as the benchmark, a comparison is made with the prediction errors based on virtual mirror and monitoring data, and the comparison results are shown in Table 7.

As shown in Table 7, the digital twin-driven prediction method exhibits lower MAE and RMSE values. In the 0–180 h stage, the MAE reductions relative to both virtual mirror and monitoring data exceed 47%, while the RMSE reductions surpass 53%. In the 0–360 h stage, both MAE and RMSE still achieve reductions of over 16%. These results

demonstrate that the prediction accuracy and stability achieved by fusing twin data are significantly superior to those obtained using either virtual mirror data or monitoring data alone, effectively improving the remaining useful life prediction accuracy and validating the feasibility of the proposed method.

Table 6. Comparison of prediction errors across different methods.

Time Range (h)	Metric	Digital Twin	Virtual Mirror	Monitoring Data
0–180	MAE	37.8	72.2	86.6
	RMSE	45.4	72.2	57.4
0–360	MAE	38.86	83.83	90.67
	RMSE	56.66	83.83	67.81

Table 7. Error reduction ratios of the digital twin-driven method relative to other methods.

Time Range (h)	Relative to Virtual Mirror		Relative to Monitoring Data	
	MAE Reduction	RMSE Reduction	MAE Reduction	RMSE Reduction
0–180	47.6%	53.6%	50.5%	57.1%
0–360	37.1%	32.4%	20.9%	16.4%

7. Conclusions

This paper addresses the problem of real-time precision remaining useful life (PRUL) prediction for CNC rotary tables. A five-dimensional digital twin framework was established. Based on the Meta-action unit theory, a theoretical PRUL prediction model incorporating both initial errors and time-varying errors was proposed. The data acquisition requirements for the physical entity were clarified, and correction rules for model parameters driven by digital twin data were formulated, thereby realizing a real-time PRUL prediction service for CNC rotary tables. Case study results demonstrate that the proposed method can provide an effective model foundation for predictive maintenance. The main conclusions are as follows:

(1) By modeling the initial precision and time-varying errors of the CNC rotary table, and solving the Wiener process model parameters using historical data from similar products, a theoretical PRUL prediction model for the CNC rotary table was obtained. This model is capable of predicting the PRUL in the absence of real-time monitoring data; however, the prediction results are insufficiently accurate.

(2) Under conditions where the amount of real-time monitoring data is limited, the prediction results driven solely by monitoring data exhibit considerable deviations. In contrast, the twin data generated by fusing theoretical model data with monitoring data can correct parameters within the model, thereby effectively improving prediction accuracy. As shown in Table 7, the prediction errors based on twin data are substantially lower than those of either virtual mirror data or monitoring data. Particularly in the 0–180 h stage, all error reduction rates approach or exceed 50%. In the 0–360 h stage, even as the amount of monitoring data increases, the twin data method still maintains error reductions of over 16%. These results indicate that twin data-driven prediction overcomes the limitations of relying on a single data source (either a physical model or monitoring data), while also enhancing the accuracy and stability of remaining useful life prediction, thereby validating the effectiveness of the proposed method.

(3) The digital twin-driven prediction method integrates real-time monitoring data, enabling accurate real-time predictions based on the output precision data of each individual CNC rotary table, thereby providing a basis for customized maintenance. In addition,

considering that CNC rotary tables often involve multiple precision indicators, future research will analyze the coupling relationships among these indicators and establish a PRUL prediction model covering multiple indicators, so as to further enhance the applicability of the method.

(4) The effectiveness of this method has been validated on the CNC rotary table, and its core concept can be extended to other complex mechanical structures. By integrating simulation data with measured data and establishing a digital twin framework, it is expected to achieve accurate PRUL prediction for different mechanical structures, thereby enhancing the generality and engineering application value of the proposed method.

Furthermore, the present study has certain limitations. Due to the limited scale of currently available monitoring data for CNC rotary tables, a relatively conservative fusion strategy (e.g., arithmetic averaging) was adopted when integrating the physical model with real-time data, rather than employing more precise fusion approaches such as adaptive weighting. In future work, as monitoring data continue to accumulate, adaptive weighting-based fusion methods will be explored to further improve prediction accuracy. On the other hand, accurate thermal deformation analysis of gear meshing and worm gear pairs remains challenging. Constrained by computational complexity, the present study did not adopt a high-precision thermal deformation analysis method, which may affect the prediction accuracy of the PRUL of CNC rotary tables to some extent. Future research will explore PRUL prediction methods that balance computational efficiency with thermal deformation analysis accuracy.

Author Contributions: Z.M. and H.W. compiled the manuscript, F.X. was in charge of the whole trial, and an engineering example was studied by G.Z. All authors have read and agreed to the published version of the manuscript.

Funding: This work is supported by the Natural Science Foundation of Chongqing, China (Chongqing Municipal Science and Technology Bureau, CSTB2025NSCQ-GPX0329); Special Funding for Postdoctoral Research Projects in Chongqing (Chongqing Municipal Human Resources and Social Security Bureau, 2023CQBSHTB3153); The Science and Technology Research Program of Chongqing Municipal Education Commission (Grant No. KJQN202401326; KJQN202501331); Chongqing University of Arts and Sciences sponsors research projects (Chongqing University of Arts and Sciences, R2022ZZ02); Natural Science Foundation Project of Yongchuan District, Chongqing (Chongqing Yongchuan District Science and Technology Bureau, 2023yc-jckx20049); and Opening Project of Engineering Research Center of Chongqing Education Commission of China in Running and Maintenance of Robots, Engineering Research Center of Chongqing Education Commission of China in Running and Maintenance of Robots (YWZX20260004).

Data Availability Statement: The original contributions presented in this study are included in the article. Further inquiries can be directed to the corresponding author.

Acknowledgments: The authors sincerely thank everyone whose constructive comments and valuable suggestions have significantly improved the quality of this manuscript.

Conflicts of Interest: The authors declare no conflicts of interest.

Abbreviations

The following abbreviations are used in this manuscript:

PRUL	Precision Remaining Useful Life
RUL	Remaining Useful Life
MAU	Meta-action Unit
MAE	Mean Absolute Error
RMSE	Root Mean Square Error

Appendix A

Table A1. Terminology in the paper.

Term	Definition
Precision Remaining Useful Life (PRUL)	The remaining time before the output precision of the CNC rotary table first reaches the precision failure threshold.
Precision Failure Threshold	The critical precision value at which the CNC rotary table is considered to have failed.
Indexing Positioning Accuracy	The output precision indicator of the CNC rotary table during indexing positioning
Model-Driven Method	A prediction method that relies on physical empirical models to establish theoretical performance degradation curves.
Data-Driven Method	A prediction method that analyzes real-time data using stochastic process models or deep learning approaches.
Hybrid-Driven Method	A prediction method that fuses physical models with data-driven methods.
Wiener Process Model	A stochastic process model used to describe the random degradation of the output precision of a mechanical system.
Virtual Mirror	A virtual model that characterizes the theoretical precision degradation law of the CNC rotary table using numerical simulation and physical mechanism models.
Physical Entity	The actual CNC rotary table in operation along with its sensing and monitoring system, responsible for real-time data acquisition.
Data Center	The central module for storing and managing data generated by the virtual mirror and collected by the physical entity.
Connection System	The system enabling data communication among modules through information transmission methods and interface protocols.
Service System	The system that outputs prediction results from the digital twin framework and provides a basis for subsequent decision-making.
Twin Data	Corrected data generated by fusing virtual mirror data with physical entity monitoring data.
Meta-action Unit (MAU)	The smallest motion unit in a mechanical system decomposed according to the motion transmission path, consisting of five major components.
Meta-action Theory	A structured decomposition method that decomposes a mechanical system into Meta-action units according to the motion transmission path.
Power Input Component	The component that receives external power (torque or motion) and introduces it into the Meta-action unit.
Intermediate Component	The transmission component located between the power input component, power output component, and support component in a Meta-action unit.
Power Output Component	The component in a Meta-action unit that directly outputs motion.
Support Component	The component in a Meta-action unit that provides structural support.
Fastener	A component used to secure and connect other parts within a Meta-action unit, preventing relative movement.
Initial Precision Model	A mathematical model of the initial assembly precision of the CNC rotary table established based on Meta-action theory.
Error Propagation Path	The cumulative path of component geometric errors along the assembly sequence and motion transmission sequence.
Error Accumulation	The progressive superposition of component-level errors along the assembly sequence and unit-level errors along the motion transmission sequence.
Intra-MAU Error Accumulation	The superposition of geometric errors of components within a Meta-action unit along the assembly sequence.

Table A1. *Cont.*

Term	Definition
Inter-MAU Error Accumulation	The superposition of errors between Meta-action units along the motion transmission sequence.
Mean Absolute Error (MAE)	The average of the absolute differences between predicted and actual values.
Root Mean Square Error (RMSE)	The square root of the mean of the squared errors between predicted and actual values.

Table A2. Symbols in the paper.

Symbol	Description
Δx, Δy, Δz	Small translational deviations along x, y, z directions
$\Delta\alpha$, $\Delta\beta$, $\Delta\gamma$	Small rotational deviations about α, β, γ axes
E_{1r}	Geometric error of power input component
E_{2is}	Geometric error of support component
E_{3jo}	Geometric error of intermediate component
E_{4u}	Geometric error of power output component
E_{MAU}	Output precision of Meta-action unit
$P_x^{(A_1)}$	Output accuracy of Gear MAU in x direction
$P_x^{(A_2)}$	Output accuracy of Worm MAU in x direction
$P_x^{(A_3)}$	Output accuracy of Worktable MAU in y direction
P_R	Initial assembly accuracy of CNC rotary table
T	Temperature field function of the worm gear pair
λx, λy, λz	Thermal conductivity in each direction
ϕ	Internal heat source
ρ	Material density
c	Specific heat capacity
q_m	Instantaneous frictional heat flux
f	Friction coefficient
p	Contact stress
v_s	Relative sliding velocity
h_m	Convective heat transfer coefficient at tooth meshing zone
T_m	Medium temperature for convective heat transfer in the tooth meshing zone
h_s	Convective heat transfer coefficient of non-working zone
T_s	Medium temperature for convective heat transfer in the non-working area
β	Heat partition coefficient
λ_1, λ_2	Thermal conductivity of worm wheel and worm materials
ρ_1, ρ_2	Density of worm wheel and worm materials
c_1, c_2	Specific heat of worm wheel and worm materials
v_{1t}, v_{2t}	Relative tangential velocities of worm wheel and worm at meshing point
e_{hw}	Thermal strain of worm wheel
e_{hg}	Thermal strain of worm
$\Delta h(t)$	Wear amount at each infinitesimal time step
k	Wear coefficient
q	Half-width of Hertz contact zone
Δt	Infinitesimal time interval
v_{ws}	Relative motion velocity of worm wheel
d_1	Pitch diameter of worm
n_1	Rotational speed of worm
γ	Lead angle
p_w	Contact stress between worm and worm wheel
K	Load factor
T_2	Torque of worm wheel
m	Module of worm
Z_2	Number of worm wheel teeth
Δh_w	Wear amount at each contact instant
$\widetilde{n}$	Rotational speed of CNC rotary table
$e_{ww}(t)$	Total wear amount on worm wheel tooth surface

Table A2. *Cont.*

Symbol	Description
N_1	Pressure on inner raceway
N_2	Support force on outer raceway
f_1, f_2	Friction forces
F_k^1, F_k^2	Forces exerted by the cage on the rollers
p_g	Contact stress between roller and raceway
q_g	Half-width of bearing Hertz contact zone
R_1	Contact circle diameter of inner raceway
v_{gs}	Relative velocity between roller and raceway
$e_{gw}(t)$	Wear amount of rotary table bearing
R_0	Roller diameter
z	Number of rollers
Δh_1, Δh_2, Δh_3	Wear amount per contact of inner raceway, roller, and outer raceway
$X(t)$	Output accuracy (Wiener process)
x_0	Initial output accuracy
μ	Drift coefficient (degradation rate)
σ_B	Diffusion coefficient (uncertainty level)
$B(t)$	Standard Brownian motion
ξ	Precision threshold of the CNC rotary table
T_{RUL}	Precision remaining precision useful life
x_{ti}	Output accuracy at time t_i
x_{0d}	Initial precision value of the CNC rotary table
μ_{P}	Fitted drift coefficient
$\overline{x}$	Mean value of the precision data
$\overline{t}$	Mean value of the time data
μ_v	Drift coefficient calculated from the virtual simulation
μ_d	Corrected drift coefficient
σ_{Bp}	Diffusion coefficient obtained by real-time monitoring data
σ_{Bv}	Diffusion coefficient obtained by substituting historical data
σ_{Bd}	Corrected diffusion coefficient

Appendix B

Table A3. The error forms of parts.

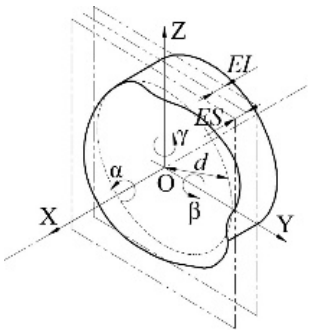
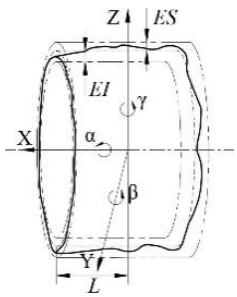
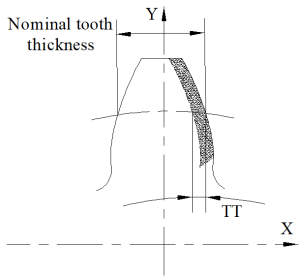
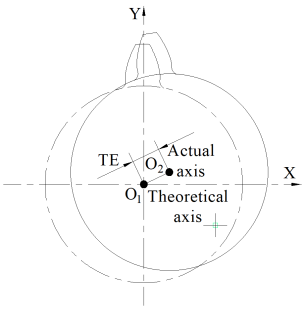
Error Form	Error Schematic Diagram	Error Model
Planar-type error		$\mathbf{T}_p = \begin{pmatrix} 1 & -\Delta\gamma & \Delta\beta & \Delta x \\ \Delta\gamma & 1 & 0 & 0 \\ -\Delta\beta & 0 & 1 & 0 \\ 0 & 0 & 0 & 1 \end{pmatrix}$
Cylindrical-type error		$\mathbf{T}_c = \begin{pmatrix} 1 & -\Delta\gamma & \Delta\beta & 0 \\ \Delta\gamma & 1 & 0 & \Delta y \\ -\Delta\beta & 0 & 1 & \Delta z \\ 0 & 0 & 0 & 1 \end{pmatrix}$

Table A3. *Cont.*

Error Form	Error Schematic Diagram	Error Model
Gear-type errors		$\mathbf{T}_T = \begin{pmatrix} 1 & 0 & 0 & \Delta x \\ 0 & 1 & 0 & 0 \\ 0 & 0 & 1 & 0 \\ 0 & 0 & 0 & 1 \end{pmatrix}$
		$\mathbf{T}_E = \begin{pmatrix} 1 & 0 & 0 & \Delta x \\ 0 & 1 & 0 & \Delta y \\ 0 & 0 & 1 & 0 \\ 0 & 0 & 0 & 1 \end{pmatrix}$

Appendix C

Table A4. Distribution of geometric error parameters for each Meta-action unit.

MAU	Part	Error	Tolerance Range (μm)	Distribution Parameters	Number of Error Components
Gear MAU	Motor board $P_1^{(A1)}$	Diameter of hole $E_{11}^{(A1)}$	[0, 15]	N(7.5, 6.25)	Cylindrical-type error (4 components)
		Position of threaded hole $E_{12}^{(A1)}$	[−5, 5]	N(0, 2.78)	Special analogous error (1 component)
	Woodruff key $P_2^{(A1)}$	Height $E_{21}^{(A1)}$	[−10, 0]	N(−5, 6.94)	Special analogous error (1 component)
	Motor gear $P_3^{(A1)}$	Tooth thickness error $E_{31}^{(A1)}$	[0, 10]	N(5, 2.78)	Gear-type error (1 component)
		Eccentricity $E_{32}^{(A1)}$	[−10, 10]	N(0, 11.11)	Gear-type error (2 components)
Worm MAU	Gear $P_1^{(A2)}$	Diameter of gear hole $E_{11}^{(A2)}$	[0, 15]	N(7.5, 6.25)	Cylindrical-type error (4 components)
		Tooth thickness error $E_{12}^{(A2)}$	[0, 10]	N(5, 2.78)	Gear-type error (1 component)
		Eccentricity $E_{13}^{(A2)}$	[−10, 10]	N(0, 11.11)	Gear-type error (2 components)
	Thrust ball bearing $P_2^{(A2)}$	Outside diameter $E_{21}^{(A2)}$	[−16, 0]	N(−8, 17.78)	Cylindrical-type error (4 components)
		Inner diameter $E_{22}^{(A2)}$	[−12, 0]	N(−6, 10)	Cylindrical-type error (4 components)
	Box $P_3^{(A2)}$	Diameter of left inner hole $E_{31}^{(A2)}$	[−13, 3]	N(−5, 7.11)	Cylindrical-type error (4 components)
		Diameter of right inner hole $E_{32}^{(A2)}$	[0, 15]	N(7.5, 6.25)	Cylindrical-type error (4 components)

Table A4. *Cont.*

MAU	Part	Error	Tolerance Range (μm)	Distribution Parameters	Number of Error Components
Worm MAU	Bearing ring $P_4^{(A2)}$	Outside diameter $E_{41}^{(A2)}$	[−19, 0]	N(−9.5, 25.03)	Cylindrical-type error (4 components)
		Inner diameter $E_{42}^{(A2)}$	[−13, 3]	N(−5, 7.11)	Cylindrical-type error (4 components)
		Concentricity of inner ring and outer ring $E_{43}^{(A2)}$	[0, 3]	N(1.5, 0.25)	Cylindrical-type error (4 components)
	Needle bearing $P_5^{(A2)}$	Outside diameter $E_{51}^{(A2)}$	[−25, 0]	N(−12.5, 43.40)	Cylindrical-type error (4 components)
		Inner diameter $E_{52}^{(A2)}$	[−12, 0]	N(−6, 10)	Cylindrical-type error (4 components)
	worm $P_6^{(A2)}$	Concentricity of second shaft segment from the left $E_{61}^{(A2)}$	[0, 3]	N(1.5, 0.25)	Cylindrical-type error (4 components)
		Concentricity of first shaft segment from the right $E_{62}^{(A2)}$	[0, 5]	N(2.5, 0.69)	Cylindrical-type error (4 components)
		Diameter of first shaft segment from the right $E_{63}^{(A2)}$	[−4.5, 4.5]	N(0, 2.25)	Cylindrical-type error (4 components)
		Radial circular runout of worm reference circle $E_{64}^{(A2)}$	[0, 3]	N(1.5, 0.25)	Special analogous error (1 component)
Worktable MAU	Box $P_1^{(A3)}$	Diameter of box hole $E_{11}^{(A3)}$	[0, 20]	N(10, 11.11)	Cylindrical-type error (4 components)
	Turntable bearing $P_2^{(A3)}$	Inner diameter $E_{21}^{(A3)}$	[−13, 0]	N(−6.5, 10.69)	Cylindrical-type error (4 components)
		Outside diameter $E_{22}^{(A3)}$	[−15, 0]	N(−7.5, 14.06)	Cylindrical-type error (4 components)
	Turntable spindle $P_3^{(A3)}$	Diameter of right shaft segment $E_{31}^{(A3)}$	[−18, 0]	N(−9, 20.25)	Cylindrical-type error (4 components)
		Concentricity of right shaft segment $E_{32}^{(A3)}$	[0, 10]	N(5, 2.78)	Cylindrical-type error (4 components)
		Diameter of first shaft segment from the left $E_{33}^{(A3)}$	[−22, 0]	N(−11, 30.25)	Cylindrical-type error (4 components)
		Diameter of second shaft segment from the left $E_{34}^{(A3)}$	[−10, 0]	N(−5, 6.94)	Cylindrical-type error (4 components)
	Worm wheel $P_4^{(A3)}$	Diameter of worm wheel hole $E_{41}^{(A3)}$	[0, 25]	N(12.5, 17.36)	Cylindrical-type error (4 components)
		Tooth thickness error $E_{42}^{(A3)}$	[0, 10]	N(5, 2.78)	Gear-type error (1 component)
		Eccentricity $E_{43}^{(A3)}$	[−10, 10]	N(0, 11.11)	Gear-type error (2 components)
	Worktable $P_5^{(A3)}$	Diameter of worktable hole $E_{51}^{(A3)}$	[0, 15]	N(7.5, 6.25)	Cylindrical-type error (4 components)

(It should be noted that when the errors of a small number of components cannot be directly classified into cylindrical, planar, or gear types based on their actual geometric form, they can be categorized by analogy according to the key feature dimensions and assembly functions of the components. For example, the threaded-hole position error, the semicircular-key height error, and the circular runout error are all specified by a single tolerance value representing the maximum allowable deviation magnitude. These errors do not require decomposition into multiple directional components and are therefore treated as a single component within the screw theory framework. In addition, when multiple geometric tolerances jointly constrain the same feature, the tighter tolerance zone governs that feature dimension).

Appendix D

Table A5. The material parameters of the worm and worm wheel.

Part	Material Grade	Thermal Conductivity (W/(m·k))	Density (g/cm^3)	Specific Heat Capacity (J/(kg·k))	Linear Velocity of Meshing Point (m/s)
Worm	20Cr	$\lambda_1 = 46.4$	$\rho_1 = 7.83$	$c_1 = 502.4$	$v_{1t} = 0.995$
Worm wheel	ALBC2	$\lambda_2 = 71.2$	$\rho_2 = 7.75$	$c_2 = 436.7$	$v_{2t} = 0.0524$

Table A6. The parameters of bearings.

Item	Bearing Type	Inner Diameter	Outside Diameter	Thickness
Single-direction thrust ball bearing 1	51,205/P5	25 mm	47 mm	15 mm
Single-direction thrust ball bearing 2	51,106/P5	30 mm	47 mm	11 mm
Needle bearing 1	NK25/20	25 mm	33 mm	20 mm
Needle bearing 2	NK24/20	24 mm	32 mm	20 mm
Turntable bearing	YRT120	120 mm	210 mm	40 mm

Table A7. The structural parameters of the CNC rotary table.

Worm Gear Pair			
Item	**Value**	**Item**	**Value**
Worm gear pair type	ZI	Hand	Right
Teeth number of worm gear	90	Module (mm)	2
Transmission ratio	90	Lead angle	3°4′23″
Number of threads	1	Pressure angle	15°
Worm gear pitch diameter (mm)	180	Worm pitch diameter (mm)	38
Torque (N·m)	180	Speed (rpm)	11.1
Gear pair			
Item	**Value**	**Item**	**Value**
Module (mm)	2	Transmission ratio	2
Pressure angle	20°	Tooth thickness (mm)	16
Teeth of driving gear	24	Teeth of driven gear	48

Box					
Item	**Value**	**Item**	**Value**	**Item**	**Value**
Length (mm)	286	Width (mm)	163	Height (mm)	300

Bearing spacing	
Item	**Value**
worm bearing span (mm)	150

References

1. Ullah, A.; Chan, T.C.; Chang, S.L. An integrated dynamic modeling and stiffness compensation approach for precision roller rotary table machine. *Int. J. Adv. Manuf. Technol.* **2025**, *139*, 1723–1736. [CrossRef]
2. Gultekin, E.; Aktas, M.S. Toward Proactive Maintenance: A Multi-Tiered Architecture for Industrial Equipment Health Monitoring and Remaining Useful Life Prediction. *Int. J. Softw. Eng. Know.* **2024**, *34*, 1831–1856. [CrossRef]
3. Zhou, N.; Wei, H.F.; Jiang, H.Y.; Cheng, Y.; Yao, Y.M.; Huang, P.; Zhang, W.H. Fatigue crack propagation model and life prediction for pantographs on High-Speed trains under different service environments. *Eng. Fail. Anal.* **2023**, *149*, 107065. [CrossRef]

4. Manouchehrynia, R.; Abdullah, S.; Singh, S.S.K.; Correia, J.A.F.O. Reliability-based fatigue life assessment using random road load condition and local damage criteria. *Eng. Fail. Anal.* **2023**, *146*, 107157. [CrossRef]
5. Yuan, R.; Chen, R.T.; Li, H.Q.; Yang, W.K.; Li, X.X. Dynamic Reliability Evaluation and Life Prediction of Transmission System of Multi-Performance Degraded Wind Turbine. *Cmes-Comp. Model. Eng.* **2023**, *135*, 2331–2347. [CrossRef]
6. Huang, M.Q.; Du, Z.Y.; Lu, R.B.; Wang, X.J.; Peng, C.H. A framework for state assessment and remaining useful life prediction of control rod drive mechanism roller. *Nucl. Eng. Des.* **2025**, *445*, 114460. [CrossRef]
7. Chang, Y.; Tang, H.S.; Ren, Y.; Anil, K. Hybrid data and failure mechanism model-driven method for predicting the remaining useful life of axial piston pump. *J. Braz. Soc. Mech. Sci.* **2025**, *47*, 418. [CrossRef]
8. Chen, Z.; Ran, Q.; Chen, N.P.; Zhang, Y.; Tang, J.; Sun, Y.B.; Liu, Z.; Hou, J.C. Spatio-temporal MLP model incorporating physical-informational neural networks for remaining useful life prediction. *Mech. Syst. Signal Process.* **2026**, *244*, 113815. [CrossRef]
9. Ma, D.; Li, J.K.; Feng, Q.B.; He, Q.X.; Ding, Y.W.; Cui, J.Y. Simultaneous Measurement Method and Error Analysis of Six Degrees of Freedom Motion Errors of a Rotary Axis Based on Polyhedral Prism. *Appl. Sci.* **2021**, *11*, 3960. [CrossRef]
10. Chen, J.J.; Yu, M.; Zhang, B.; Zhu, R.S. Remaining Useful Life Prediction for Hybrid Systems Under Intermittent Fault Using Doubly Stochastic Process Model. *IEEE Trans. Autom. Sci. Eng.* **2025**, *22*, 16616–16631. [CrossRef]
11. Wang, Z.F.; Tao, J.L.; Hu, Y.M.; Zhang, J.Y.; Ma, L.H.; Xu, M. A multi-scale fuel cell degradation prediction method based on isometric convolution block and long short-term memory networks. *Int. J. Hydrogen Energy* **2024**, *69*, 675–686. [CrossRef]
12. Gürsoy, M.I. Short and long-term prognostics of the remaining useful life of a proton exchange membrane fuel cell using deep learning and transformer model. *Int. J. Hydrogen Energy* **2025**, *143*, 1120–1132. [CrossRef]
13. Liu, Z.M.; Lei, Z.H.; Wen, G.R.; Wang, E.X.; Su, Y.; Zhang, Z.F.; Chen, X.F. Self-data-driven remaining useful life prediction of rotating machinery under time-varying operating conditions based on a two-stage hybrid state-space model. *Reliab. Eng. Syst. Saf.* **2026**, *268*, 111981. [CrossRef]
14. Yi, J.M.; Ma, C.B.; Wang, H. A Data-Driven Remaining Useful Life Prediction Method for Power MOSFETs Considering Nonlinear Dynamical Behaviors. *IEEE Trans. Electron Devices* **2025**, *72*, 1885–1892. [CrossRef]
15. Duan, Y.H.; Liu, Z.; Li, H.H.; Zhang, C.; Zhang, N. A hybrid-driven remaining useful life prediction method combining asymmetric dual-channel autoencoder and nonlinear Wiener process. *Appl. Intell.* **2023**, *53*, 25490–25510. [CrossRef]
16. Wang, Z.D.; Shi, H.T.; Wu, R.Y. A physics-data hybrid driven method for predicting the remaining useful life of rolling bearings. *Meas. Sci. Technol.* **2026**, *37*, 105104. [CrossRef]
17. Tao, F.; Zhan, H.; Liu, A.; Nee, A.Y.C. Digital Twin in Industry: State-of-the-Art. *IEEE Trans. Ind. Inform.* **2019**, *15*, 2405–2415. [CrossRef]
18. He, D.Q.; Zhao, J.Y.; Jin, Z.Z.; Huang, C.G.; Zhang, F.; Wu, J.X. Prediction of bearing remaining useful life based on a two-stage updated digital twin. *Adv. Eng. Inform.* **2025**, *65*, 103123. [CrossRef]
19. Cui, L.; Xiao, Y.C.; Liu, D.D.; Han, H.G. Digital twin-driven graph domain adaptation neural network for remaining useful life prediction of rolling bearing. *Reliab. Eng. Syst. Saf.* **2024**, *245*, 109991. [CrossRef]
20. Lu, Q.B.; Li, M. Digital Twin-Driven Remaining Useful Life Prediction for Rolling Element Bearing. *Machines* **2023**, *11*, 678. [CrossRef]
21. Lu, Q.B.; Zhu, D.; Wang, M.; Li, M. Digital Twin-Driven Thermal Error Prediction for CNC Machine Tool Spindle. *Lubricants* **2023**, *11*, 219. [CrossRef]
22. Yang, B.; Zhang, G.B.; Ran, Y.; Yu, H. Kinematic modeling and machining precision analysis of multi-axis CNC machine tools based on screw theory. *Mech. Mach. Theory* **2019**, *140*, 538–552. [CrossRef]
23. Li, J.F.; Gu, M.H.; Li, Y.L.; Wen, S.T.; Zhang, G.B. Predictive analysis of the precision remaining useful life of CNC machine tools based on Meta-action unit. *Proc. Inst. Mech. Eng. Part B-J. Eng. Manuf.* **2025**, *239*, 185–197. [CrossRef]
24. Louhichi, B.; Slamani, M. Meta-action Unit-Based Modeling of Accuracy Stability, Error Propagation and Intelligent Compensation in CNC Machine Tools: A Comprehensive Review Toward Industry 4.0 and 5.0. *Machines* **2026**, *14*, 874. [CrossRef]
25. Tao, F.; Liu, W.R.; Zhang, M.; Hu, T.L.; Qi, Q.L.; Zhang, H.; Sui, F.Y.; Wang, T.; Xu, H.; Huang, Z.G.; et al. Five-dimension digital twin model and its ten applications. *Comput. Integr. Manuf. Syst.* **2019**, *25*, 1–18.
26. Minguzzi, E. A geometrical introduction to screw theory. *Eur. J. Phys.* **2013**, *34*, 613–632. [CrossRef]
27. Chen, Y.F. A reliability allocation method for mechanical products considering Meta-action performance factors and failure correlation. *Qual. Reliab. Eng. Int.* **2025**, *41*, 732–746. [CrossRef]
28. Li, L.W.; Zhang, H.L.; Ren, X.M. A Modified Multi-innovation Algorithm to Turntable Servo System Identification. *Circuits Syst. Signal Process.* **2020**, *39*, 4339–4353. [CrossRef]
29. Janakiraman, V.; Li, S.; Kahraman, A. An Investigation of the Impacts of Contact Parameters on Wear Coefficient. *J. Tribol.* **2014**, *136*, 69–74. [CrossRef]
30. Zhang, X.G.; Chen, W.; Wang, H.W.; Zhang, W.; Mu, Z.Y.; Li, J.; Ding, Z.Z. Physics-driven precision reliability prediction modelling for the condition estimation of worm gear turntable. *Precis. Eng.* **2025**, *94*, 43–53. [CrossRef]

31. Wang, H.W.; Xiang, J.W.; Zhao, X.F.; Li, Y.L. A kinematic precision reliability evaluation method for rotor-bearing systems considering multi-source wear degradations and random errors. *Int. J. Adv. Manuf. Technol.* **2023**, *124*, 4159–4173. [CrossRef]
32. Wang, G.; Chen, J.; Hong, R.J.; Wang, H. Model for the positional accuracy degradation of NC rotary tables based on the hidden Markov model and optimized particle filtering. *J. Vib. Shock* **2018**, *37*, 7–13. [CrossRef]

Disclaimer/Publisher's Note: The statements, opinions and data contained in all publications are solely those of the individual author(s) and contributor(s) and not of MDPI and/or the editor(s). MDPI and/or the editor(s) disclaim responsibility for any injury to people or property resulting from any ideas, methods, instructions or products referred to in the content.